PCR products cloned into a pGEM-T Easy vector (Promega, Madison, WI, USA) were analyzed for TCR sequences using CEQ DTCS-Quick Start Kit according to the manufacturer's protocol (Beckman Coulter Inc., Fullerton, CA, USA).

^{51}Cr release cytotoxicity assay

BALB/3T3 fibroblast line (H-2^d), J774 macrophage line (H-2^d), p815 mastocytoma line (H-2^d), EL-4 lymphoma line (H-2^b), L929 fibroblast line (H-2^k) obtained from Dainippon Sumitomo Pharma (Osaka, Japan) and synovial cells of SKG mice (H-2^d) were used as target cells. Synovial cells (1×10^4) were seeded in 96-well flat-bottom plates with 40 U/well of IFN-γ for 2 days and radiolabeled with 2.5 μCi/well of $Na_2^{51}CrO_4$ (Daiichi Radioisotope Laboratories, Ltd, Tokyo, Japan) for 2 h. Other target cells (3×10^5) were radiolabeled with 20 μCi of $Na_2^{51}CrO_4$ for 2 h and seeded in 96-well round-bottom plates at 1×10^4 cells per well. Effector cells (4×10^5) were added in each well in triplicate and incubated for 8 h. Relative cytotoxicity was calculated as follows from the radioactivity released in the culture supernatant; percent specific lysis = 100(experimental − spontaneous)/(maximal − spontaneous) counts per minute. Maximal lysis and spontaneous release were determined from target cells incubated with surfactant ×7 (Flow Laboratories, ICN Biomedicals, Inc., Aurora, OH, USA) or without effector cells, respectively.

Adoptive transfer

Spleen T cells from SKG mice or (SKG × BALB/c)F_1 mice and each SKG T cell clones (1×10^7) were intravenously transferred to C.B-17 SCID mice (8 weeks) or BALB/c-nu/nu mice (6 weeks), respectively. Control dengue 2F7 and 3F2 clone were collected 10–14 days after *in vitro* stimulation with specific peptide-pulsed irradiated (33 Gray) BALB/c spleen cells and transferred as described above. Severity of arthritis was scored weekly as previously described (14).

Clinical assessment of arthritis

Joint swelling was monitored by inspection and scored as follows: 0, no joint swelling; 0.1, swelling of one finger joint; 0.5, mild swelling of wrist or ankle and 1.0, severe swelling of wrist or ankle. Scores for all fingers and toes, wrists and ankles were totalled for each mouse (14).

Histological assessment of interstitial pneumonitis

Interstitial pneumonitis was evaluated microscopically depending on diffusely affected area: –, normal histology; +, 10–30%; ++, 30–60%; +++, >60% of the sections of the lungs showed pneumonitis.

Histology and immunohistochemistry

Tissues were fixed in 10% neutral formalin, paraffin embedded and stained with Haematoxylin & Eosin (H&E). Joints were additionally decalcified for 3 weeks in 10% EDTA in PBS before staining. For immunohistochemistry of joints, deparaffinized sections were incubated with 20% normal rabbit serum (Dako, Hamburg, Germany) in PBS for 15 min to block non-specific binding, primary rat anti-Ly-6G mAb (Gr-1, RB6-8C5; BD PharMingen) with appropriate dilutions overnight at 4°C, biotinylated polyclonal rabbit anti-rat antibody (Dako) and HRP-conjugated streptavidin (Dako). The slides were developed using diaminobenzidene (Elite Kit; Vector, Burlingame, CA, USA) and counterstained with Mayer's hematoxylin.

For immunohistochemistry of lungs, tissues were fixed in 4% phosphate-buffered PFA (pH 7.4) and embedded in Tissue-Tek OCT compound (Ted Pella, Inc., Redding, CA, USA). Cryostat sections were stained with rat mAbs to mouse CD4 (H129.19), CD8a (53-6.7), CD45R/B220 (RA3-6B2), Ly-6G (RB6-8C5) (BD PharMingen) and F4/80 (CI: A3-1) (CALTAG Laboratories, Burlingame, CA, USA) with appropriate dilutions followed by incubation with biotinylated secondary antibodies and HRP-conjugated streptavidin. The slides were developed as described above.

Southern blot analysis

The persistence of transferred clones in the recipients was assessed by Southern blot analysis. Two micrograms of total RNA of each tissue was treated with DNaseI and reverse transcribed using Superscript II (Invitrogen, Carlsbad, CA, USA). Nested PCRs were performed as described previously (24) to amplify TCR β chain of 35S or dengue 2F7 with the primers specific for V, J and C region. Ten microliters of the PCR products were separated on 2% agarose gel, transferred onto Hybond-N+ membranes (Amersham Biosciences, Piscataway, NJ, USA) according to the manufacturer's instructions. The membranes were prehybridized overnight with PerfectHyb (TOYOBO CO., Ltd, Osaka, Japan) at 54°C and hybridized with the third complementarity-determining region (CDR3)-specific probes labeled with ^{32}P-deoxyadenosine triphosphate for 3 h at 54°C. The membranes were washed in ×2 standard saline citrate (SSC) and 0.1% SDS at room temperature and ×0.2 SSC and 0.1% SDS at 37°C. RNA extracts of 35S and dengue 2F7 clones, diluted to 1% of concentration with RNA of L9 cells, were used as positive controls. The detection limits of 35S and dengue 2F7 were compared using the serial dilution of positive controls and both systems detected the RNA extract corresponding to the amount of one cell.

The sequences of PCR primers and probes are as follows; 35S: first PCR (BV8S3-1: 5′-ATA TGG TGC TGG CAA CCT TC-3′ and MCB1: 5′-AGG ATT GTG CCA GAA GGT AG-3′), second PCR (BV8S3-2: 5′-ACC AGA ACA ACG CAA GAA GAC T-3′ and MCB2: 5′-TTG TAG GCC TGA GGG TCC-3′), third PCR (BV8S3-3: 5′-TTC CTC CTG CTG GAA TTG GC-3′ and BJ1.5: 5′-TAG AAC AGA GAT CGA GTC CC-3′) and probe (5′-AGT GGG ACA GGG GGC AAC CA-3′). Dengue 2F7: first PCR (BV8S1-1: 5′-CCC AAA GTC CAA GAA GCA AG-3′ and MCB1), second PCR (BV8S1-2: 5′-GTA CAA GGC CTC CAG ACC AA-3′ and MCB2), third PCR (BV8S1-3: 5′-TGG CTT CCC TTT CTC AGA CA-3′ and BJ2.7: 5′-AAG GAG ACC TTG GGT GGA GT-3′) and probe (5′-TGC CAC CAA CGA CAA CTC CT-3′).

Results

Induction of arthritis and interstitial pneumonitis in SCID mice by the transfer of SKG splenic T cells

In our conventional housing environment, SKG mice started to develop arthritis around 2 months of age and

histologically evident mild interstitial pneumonitis around 6 months of age (14). To determine the role of T cells in SKG mouse autoimmunity, we transferred splenic T cells from 3-month-old arthritic SKG mice (without histologically evident pneumonitis or colitis) to T/B-cell-deficient C.B-17 SCID mice, which are histocompatible with SKG mice on the BALB/c background (14). Within 2 months after transfer, the recipient developed arthritis (14) and mild but histologically evident interstitial pneumonitis (Table 1, Fig. 1); they also developed mild colitis (data not shown). Similar cell transfer from non-arthritic heterozygotes of the SKG mutation failed to induce such lesions in the recipients. Age-matched SCID mice similarly maintained in our facility did not develop these lesions histologically (data not shown). The results thus indicate that SKG T cells are able to adoptively transfer arthritis and also have a potential to induce interstitial pneumonitis and colitis when transferred to SCID mice.

Establishment of T cell clones from arthritic joints

To analyze the mechanism of such T cell-mediated inflammatory tissue damage in multiple organs, we attempted to establish T cell clones from arthritic joints of SKG mice, as described in Materials and methods. Two T cell clones, designated 35S and 73S, were established in separate experiments. The clones were maintained and expanded with culture medium containing IL-2 and Con A (see Materials and methods). $CD8^+$ CTL clones specific for dengue virus NS3 protein were used as control.

Cytofluorometric analyses revealed that the 35S and 73S clones were $CD8^+$. Both expressed α and β chains of the TCR, and the expression level of the TCR on 35S was slightly lower than normal (Fig. 2). In response to *in vitro* PMA and ionomycin stimulation, 35S and 73S produced IFN-γ but no detectable amount of TNF-α, IL-4, IL-5, IL-6, IL-10 or IL-17 by ELISA (Table 2).

Clonality of each T cell line was confirmed by MHA (24) (data not shown) and sequence analysis of the TCR α and β chains with determination of the amino acid sequences of the TCRs (Table 3). Interestingly, these T cell clones shared in common the BV8S3 TCR Vβ subfamily; yet, the CDR3 sequences of the TCR β chains were different (26–29).

Table 1. Induction of arthritis, interstitial pneumonitis and colitis in SCID mice by the transfer of SKG splenic T cells

Spleen cell donor	Recipients	Arthritis	Interstitial pneumonitis	Colitis
SKG	1	++ (4.6)	++	+
	2	++ (4.0)	++	+
	3	++ (4.0)	+	+
	4	++ (3.0)	+	–
(SKG × BALB/c)F_1	1	–	–	–
	2	–	–	–
	3	–	–	–
	4	–	–	–

Cells (1×10^7) of T cells prepared from spleens of indicated mice were intravenously transferred to 8-week-old SCID mice. The severity of arthritis, interstital pneumonitis and colitis in these mice was histologically assessed 2 months later.

Autoreactivity of T cell clones

In ^{51}Cr release cytotoxicity assay to determine cytotoxic activity of the SKG clones against syngeneic synovial cells, 35S and 73S lysed SKG synovial cells prepared by crude collagenase digestion of inflamed synovium (44.0 and 16.3% of specific lysis, respectively, at a high 40:1 ratio), while control dengue 2F7 clone did not (Fig. 3A). 35S lysed not only syngeneic synovial cells but also MHC-matched cell lines, such as BALB/c-derived 3T3 cells, macrophage-like J774 cells and DBA/2 (H-2^d)-derived P815 cells, whereas the clone failed to lyse allogenic EL-4 (H-2^b) lymphoid or L929 (H-2^k) fibroblast cell line (Fig. 3B). Thus, 35S appears to recognize a ubiquitous self-peptide in an MHC-restricted manner. These

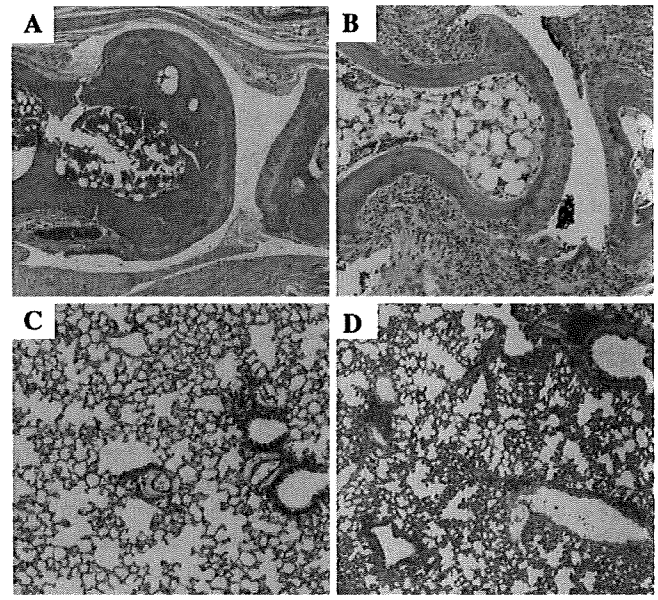

Fig. 1. Arthritis and pneumonitis in SCID mice transferred with T cells from SKG mice. Histology of a joint (A) and lung (C) of a SCID mouse T cell transferred from (SKG × BALB/c)F_1 mouse. Arthritis (B) and interstitial pneumonitis (D) in a SCID mouse T cell transferred from a SKG mouse. H&E staining (A and B, ×100; C and D, ×50).

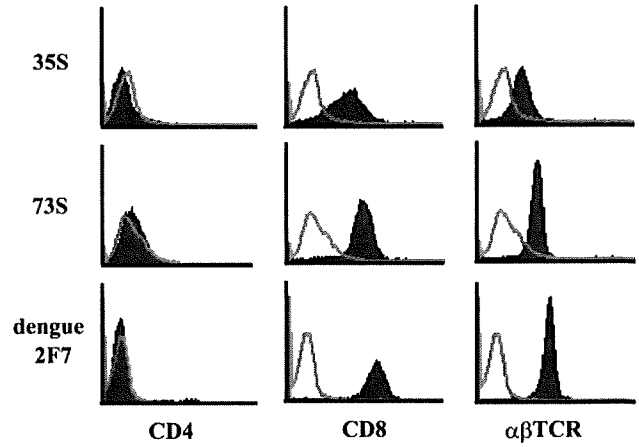

Fig. 2. Expression levels of CD4, CD8 and αβ TCR on 35S, 73S and dengue 2F7 clones.

functional characteristics, together with cell surface and cytokine-secreting profiles, indicate that 35S and 73S are CTL and that they bear self-reactive specificity.

Induction of synovitis in BALB/c nude mice by adoptive transfer of T cell clones

To examine possible arthritogenicity of the T cell clones, they were transferred to BALB/c nude mice once, and the degree of joint swelling of each recipient mouse was assessed once a week for 12 months (Fig. 4). Transfer of 35S and 73S clones induced joint swelling with incidences of 57.1% (4 out of 7 mice) and 42.9% (3 out of 7 mice), respectively, during the observation period; synovitis was histologically evident in 71.4% (5 out of 7 mice) in each transfer (Table 4, Fig. 5). Once joint swelling started in one joint following cell transfer, it slowly progressed with remissions and exacerbations, leading to swelling of other joints in a symmetrical fashion (Figs 4 and 5A–D). Two mice showed progressive debilitation to death without an apparent cause, although one of them showed dermatitis; with debilitation, joint swelling somehow remitted in these mice.

Table 2. Cytokine production (ng/ml) of T cell clones derived from SKG joints and control clones

	TNF-α	IFN-γ	IL-4	IL-5	IL-10	IL-6	IL-17
35S	0.02	180	0.03	<0.02	<0.04	0.2	<0.01
73S	0.02	80	0.03	<0.02	1.2	<0.05	<0.01
Dengue 2F7	0.2	10	ND	ND	<0.04	<0.05	<0.01
Dengue 3F2	0.02	20	ND	ND	<0.04	<0.05	<0.01

Culture supernatant of activated cells by PMA and ionomycin for 16 h were assayed by ELISA. ND, not done.

Table 3. CDR3 sequences of the TCR α and β chain used by the SKG T cell clones

TCR α chains	AV	V	N	J	AJ
35S	3S6	C A V T	S D	S G T Y Q R F	13
73S	3S1	C A A S M	R R	N S G T Y Q R F	13
Dengue 2F7	2S2/7	C A A		N Q G G R A L I F	15
Dengue 3F2	2S2/7	C A A	S G R D	Y A N K M I F	47
TCR β chains	**BV**	**V**	**N-D-N**	**J**	**BJ**
35S	8S3	C A S S G	T G G	N Q A P L F	1.5
73S	8S3	C A S S G	W G D	A E Q F F	2.1
Dengue 2F7	8S1	C A T	N D N	S Y E Q Y E	2.7
Dengue 3F2	8S2	C A S E	T R	E Q Y F	2.6

The amino acid sequences of the V, D and J regions of the TCR were determined according to the nucleotide sequences. AV and BV gene families were assigned according to Arden *et al.* (26). AJ genes were numbered according to Koop *et al.* (27). BJ genes were assigned according to Malissen *et al.* (28) and Gascoigne *et al.* (29).

Histologically, swollen joints showed marked synovial and peri-articular inflammation when examined 6–12 months after cell transfer (Fig. 5E and F). The inflammation accompanied a marked proliferation of synovial lining cells, infiltration of inflammatory cells into subsynovial tissue and joint cavity and active angiogenesis; pannus eroded the adjacent cartilage and bone (Fig. 5F). Gr-1-positive neutrophils were abundant among the infiltrating cells, as observed in the arthritic lesions of SKG mice (14, 15), whereas few T cells infiltrated into the inflammation sites (Fig. 5G and H).

In accordance with the appearance of multinuclear cells at the interface between proliferating synoviocytes and bone, many tartrate-resistant acid phosphatase-positive osteoclasts were observed in the inflamed joints (Fig. 6A–D). Safranin-O staining revealed a decrease in proteoglycan in the articular cartilage matrix of severely affected joints (Fig. 6E and F). Notably, Gr-1-positive cells, mainly neutrophils, also increased in the bone marrow (BM) of the affected recipients (Fig. 6G and H).

A high level of circulating rheumatoid factors was detected in one mouse out of seven recipients of the 35S clone and in none of the recipients of other clones (data not shown).

Some of the swollen joints following transfer of 35S $CD8^+$ clones exhibited higher expression levels of IL-17 mRNA assessed by quantitative reverse transcription (RT)–PCR than those from mice transferred with control $CD8^+$ clones (Supplementary Figure 1A, available at *International Immunology* Online), despite that 35S failed to produce IL-17 upon *in vitro* stimulation.

Taken together, the $CD8^+$ T cell clones prepared from arthritic lesions of SKG mice were able to induce arthritis in athymic nude recipients, leading to the destruction of the surrounding cartilage and the bone.

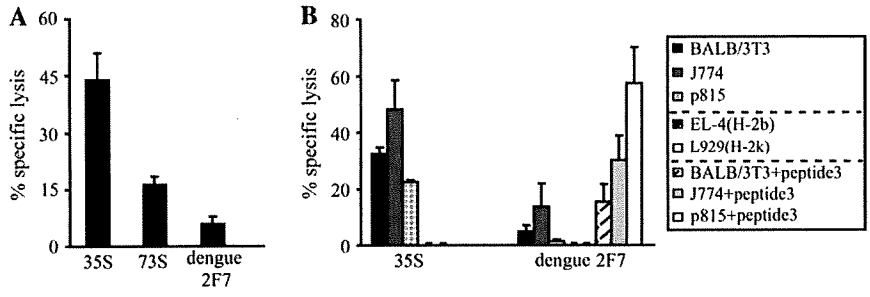

Fig. 3. *In vitro* self-reactivity of SKG T cell clones. (A) CTL activity of SKG T cell clones against SKG synovial cells. CTL clones specific for dengue virus NS3 protein, dengue 2F7, was used as control. IFN-γ-treated target cells were ^{51}Cr labeled in adherent condition and incubated with effector cells for 8 h (E:T ratio = 40). (B) CTL activity of SKG T cell clones against various types of cell lines (E:T ratio = 40). CTL activity of dengue 2F7 clone was also analyzed against H-2^d cells pulsed with a specific peptide (E:T ratio = 10). All assays were conducted in triplicate with 8 h of incubation. The mean and standard deviation of three independent experiments are shown in each bar.

Induction of interstitial pneumonitis in BALB/c nude mice by the transfer of T cell clones

Notably, histologically evident severe alveolitis and diffuse interstitial pneumonitis also developed in all the recipients of 35S and 73S but not in those recipients of dengue 2F7 and 3F2 clones (Table 4 and Fig. 7A–D). Some recipients of 35S and 73S developed only pneumonitis without histologically evident synovitis. No histologically apparent inflammation was observed in other tissues/organs including the liver and the colon in any of these recipient mice (data not shown). The diffuse pulmonary lesions (Fig. 7A and B) comprised thickening of the alveolar walls, and perivascular and peribronchiolar infiltration by inflammatory cells (Fig. 7C and D). Immunohistochemical analysis of the 73S recipients 6 months after cell transfer revealed the infiltration of a large number of granulocytes as Gr-1$^+$ cells (Fig. 7E), macrophages as F4/80$^+$ cells (Fig. 7F) and B cells as B220$^+$ cells (Fig. 7G) into the alveolar walls and spaces and also the perivascular and peribronchiolar area where only a small number of CD8$^+$ T cells were detected, which might be transferred to CD8$^+$ clones or derived from nude mice (30) (Fig. 7H). CD4$^+$ T cells were occasionally found in the lesions and could be those derived from endogenous T cells that might develop extrathymically in aged nude mice (Fig. 7I) (30).

The pulmonary tissues with severe interstitial pneumonitis following CD8$^+$ clone transfer exhibited higher expression levels of IL-17 mRNA by quantitative RT–PCR compared with the mice transferred with control CD8$^+$ clones (Supplementary Figure 1B, available at *International Immunology* Online).

Thus, the SKG arthritogenic T cell clones are able to induce interstitial pneumonitis when transferred to athymic nude mice.

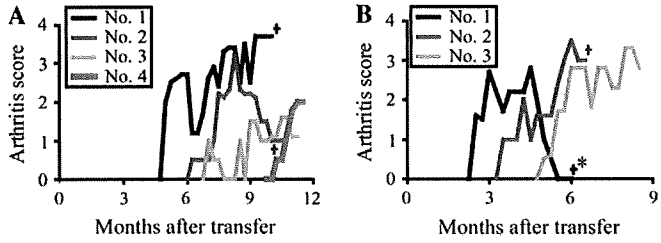

Fig. 4. Time course of joint swelling in the recipient mice of SKG T cell clones, 35S (A) and 73S (B). Score for all paws were totalized for each mouse. +, Sacrificed at the indicated time points; *, the mouse developed dermatitis at 5 months after transfer.

Detection of transferred clones in recipient mice

Since T cells were hardly detected by immunohistochemistry at the site of synovitis or pneumonitis 6 months after clone transfer (data not shown and see above), the persistence of transferred clones in the recipients was assessed by RT–PCR amplification of TCR β chain gene and Southern blot analysis of the products with a CDR3 sequence-specific probe. We adopted this method to avoid detecting nude mouse-derived oligoclonal endogenous T cells that may expand with aging (see above) (30–32). For example, a clone-specific TCR message of the 35S clone was detected in the majority of recipient spleens 1 month after transfer but not in the spleens examined 6 months later (Fig. 8). As shown in Fig. 9, the messages were

Table 4. Development of arthritis and interstitial pneumonitis in BALB/c nude mice transferred with T cell clones

Clone	Individual recipients	Macroscopically evident arthritis			Histological analysis	
		Onset (months)	Sacrifice (months)	Clinical score[a]	Synovitis[b]	Interstitial pneumonitis[c]
35S	1	5	10	3.7	++	+
	2	6	11	3.2	++	++
	3	7	11	1.6	++	+++
	4	10	12	2.0	++	+++
	5	–	9	0	+	±
	6	–	12	0	—	+++
	7	–	12	0	—	+++
73S	1	2.5	6	2.8	++	++
	2	3.5	6	3.5	++	+
	3	5	9	3.3	++	++
	4	–	8	0	+	++
	5	–	9	0	+	+++
	6	–	12	0	—	++
	7	–	12	0	—	++
Dengue 2F7	1	–	9	0	—	—
	2	–	9	0	—	—
	3	–	9	0	—	—
	4	–	9	0	—	—
	5	–	12	0	—	—
	6	–	12	0	—	—
	7	–	12	0	—	—
Dengue 3F2	1	–	12	0	—	—
	2	–	12	0	—	—

Six-week-old BALB/c nude mice were intravenously injected with 1 × 10^7 cells of each clone. The incidence of joint swelling of the recipient mice was examined weekly. Mice were sacrificed 6–12 months after cell transfer.

[a]Maximum clinical score of arthritis.

[b]–, Without change; +, microscopically observed synovitis without joint swelling; ++, macroscopically obvious joint swelling.

[c]–, Normal histology; +, 10–30%; ++, 30–60%; +++, >60% of the sections of the lungs showed pneumonitis (Fig. 7).

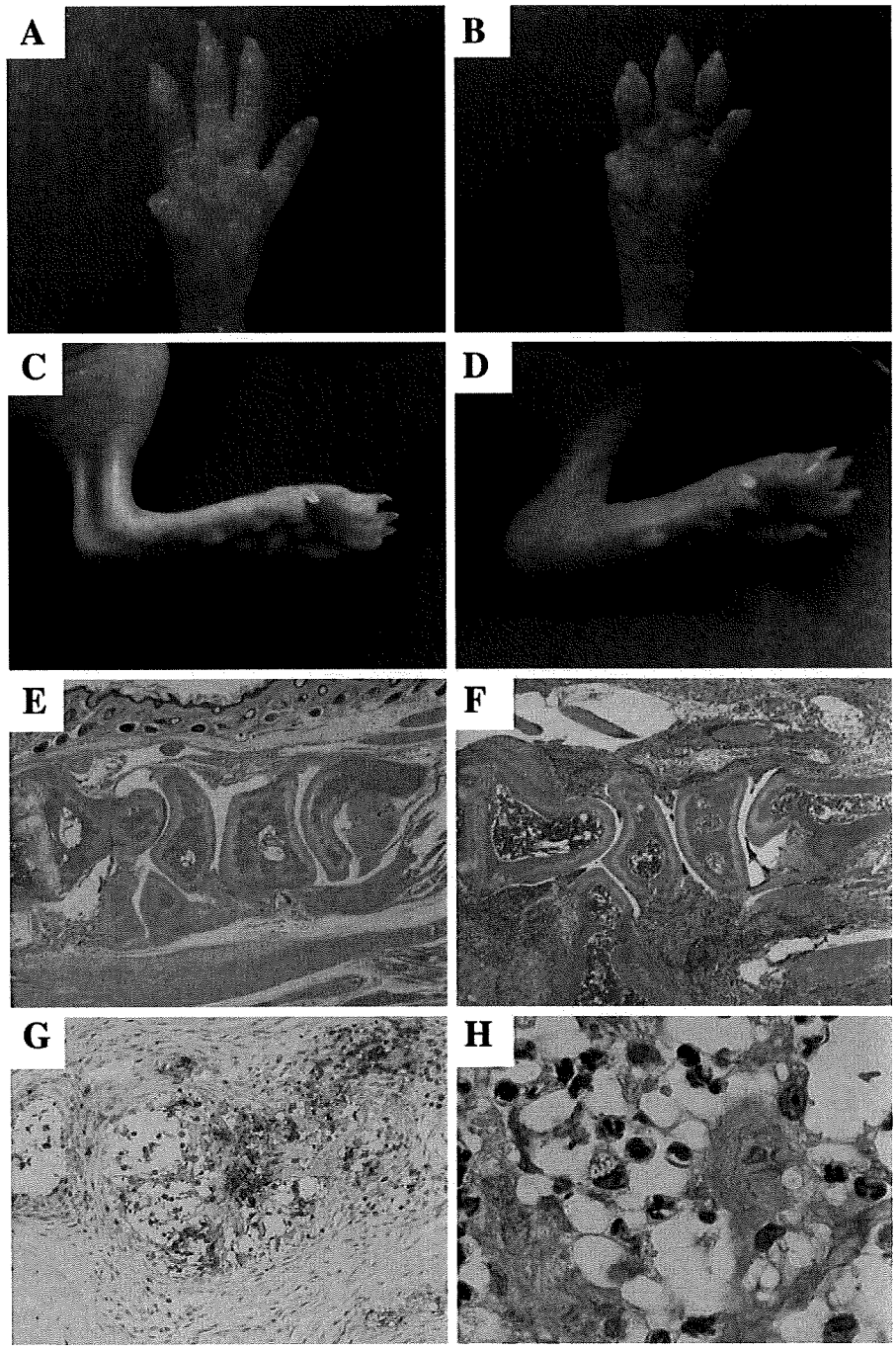

Fig. 5. Arthritis in athymic nude mice transferred with SKG T cell clones. (A–D) Macroscopic views of a forepaw (A) and a hind paw (C) of a recipient of control dengue 2F7 and a forepaw (B) and a hindpaw (D) of a recipient of 35S. (E–H) Histology of the joints of recipients of control dengue 2F7 (E) or 35S (F). Proliferation of the synovial lining cells, erosive destruction of cartilage and bone and infiltration of inflammatory cells is noted in a joint of a 35S recipient (F) (H&E staining, ×40). (G) Gr-1-positive cells were abundant among the infiltrating cells in a joint of 35S recipient mouse (×200). High-magnification view (×1000) of the synovial lesion in 35S transferred mouse, showing that most of the infiltrating cells are granulocytes or monocytes (H) (H&E staining). (A, C and E) 12 months after transfer. (B, D and F–H) 10 months after transfer.

detected in every tested tissue with high frequency for the first 3 months after cell transfer; the detection rate became lower with time; clone-specific TCR signals were not detected in most tissues examined at 6–11 months after transfer, irrespective of the swelling of the joints and the presence of interstitial pneumonitis by histological examination. These findings collectively indicate that the T cell clones initiate arthritis but the progression and persistence of the disease may not require the expansion of the clones even if a small number of them might persist in the joints and the lung.

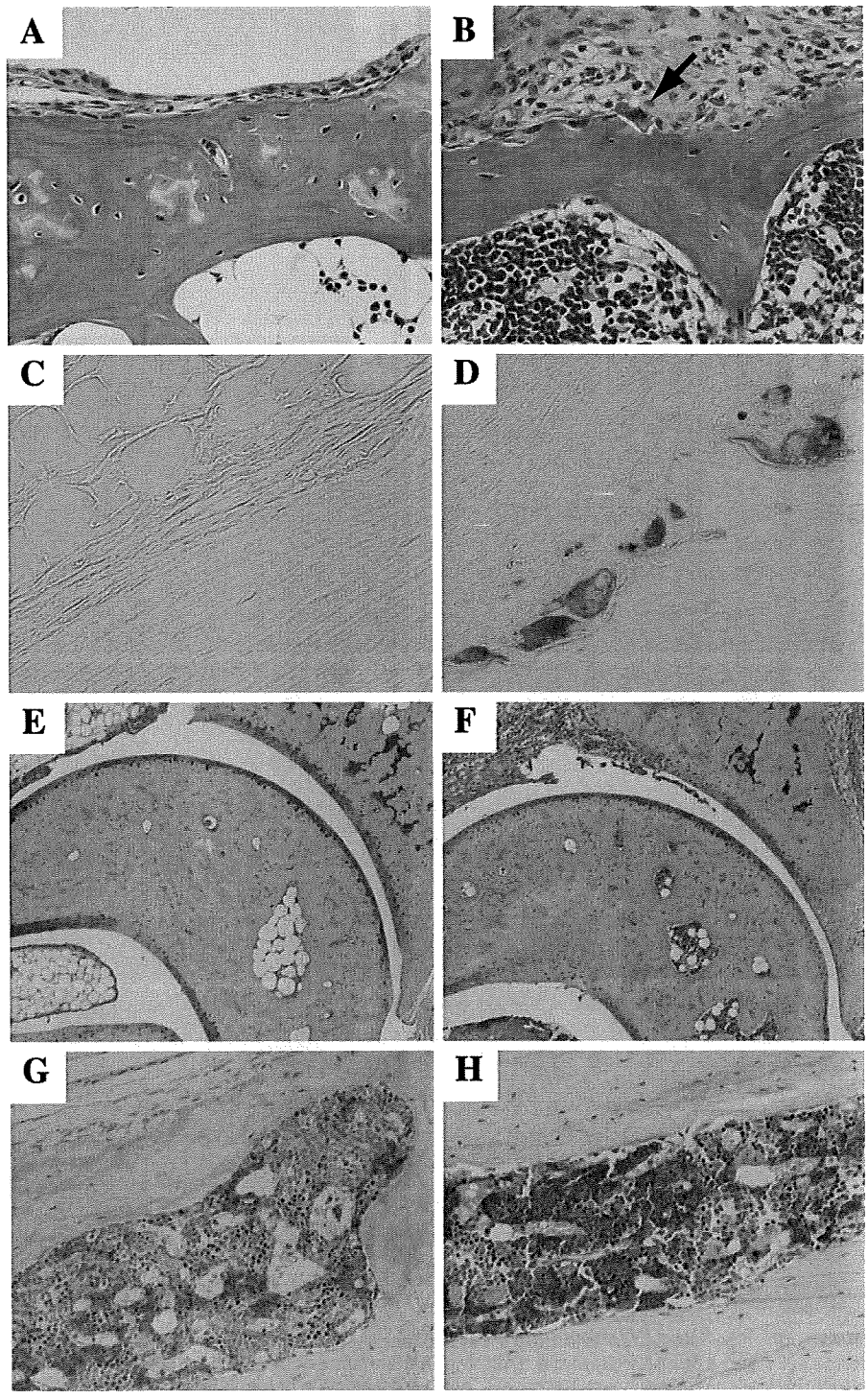

Fig. 6. Bone and cartilage destruction in athymic nude mice transferred with SKG T cell clones. High magnification of H&E-stained sections of a nude mouse recipient of dengue 2F7 (A) or 35S (B), showing bone erosion by pannus and BM activation (×400). Multinuclear cells (osteoclasts) (arrow) are also observed. Tartrate-resistant acid phosphatase-positive cells (osteoclasts) are detected in a 35S recipient (D) but not in a 2F7 recipient (C) (×400). By Safranin-O staining, proteoglycan stained red decreases in the articular cartilage matrix of a recipient of 35S (F) but not in a recipient of 2F7 (E) (×100). By immunohistochemistry, Gr-1-positive cells increase in the BM of a 35S recipient (H) but not in a 2F7 recipient (G) (×200). (A, C, E and G) 12 months after transfer; (B, D, F and H) 10 months after transfer.

Discussion

In this study, we have established two distinct $CD8^+$ T cell clones from arthritic lesions of SKG mice. Interestingly, both exhibited *in vitro* autoreactivity against not only synoviocytes but also a variety of MHC-matched cell lines and elicited both arthritis and interstitial pneumonitis when transferred to

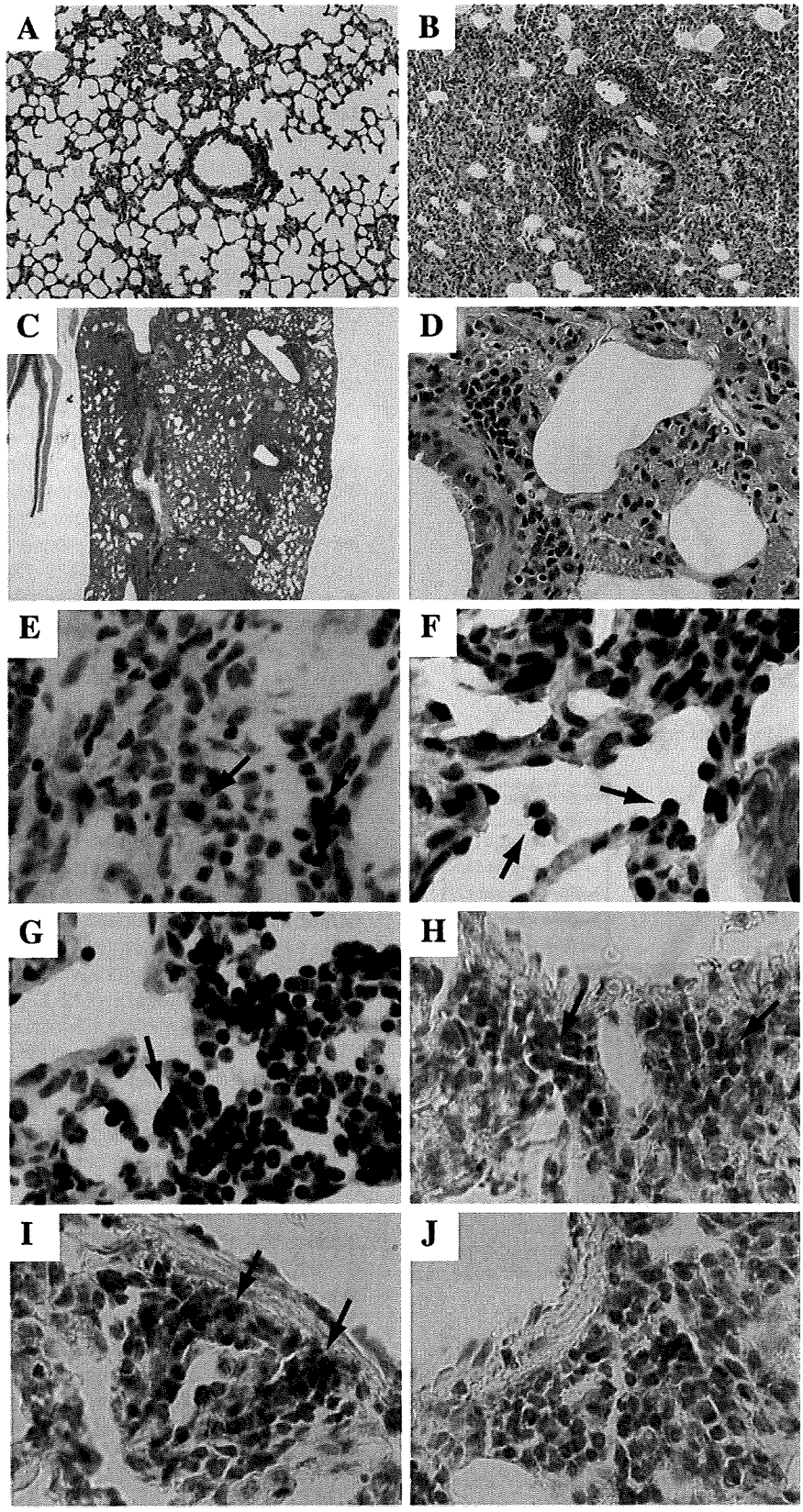

Fig. 7. Interstitial pneumonitis induced by the transfer of SKG T cell clones. (A–D) H&E-stained sections of the lungs of the recipients of control dengue 2F7 clone (A) or 73S clone (B–D) (A–B, ×100). Lower (C, ×10) and higher (D, ×400) magnification of the lung of 73S clone recipient show thickening of alveolar walls diffusely in the lung. (E–J) Serial sections of a lung of a 73S recipient mouse were stained for Ly-6G (Gr-1) (E), F4/80 (F), B220/CD45R (G), CD8a (H) or CD4 (I), with staining control (J) (×400). Typically positive cells in these stainings are arrowed. (A–J) 6 months after transfer.

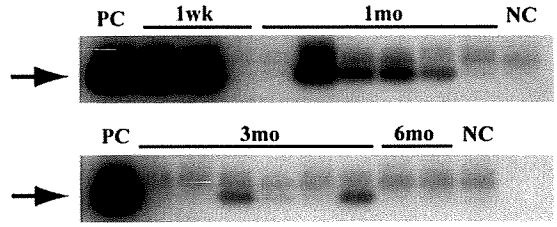

Fig. 8. Detection of a clone-specific TCR message of 35S clone in spleens by RT-PCR amplification and Southern blot analysis. After transfer of 1 × 10^7 clone cells to BALB/c nude mice, RNA was extracted from spleens at indicated days. PC, positive control (RNA from 35S clone diluted to 1%); NC, negative control (RNA from a 6-month-old non-treated BALB/c athymic nude mouse). The separate lanes represent individual mice.

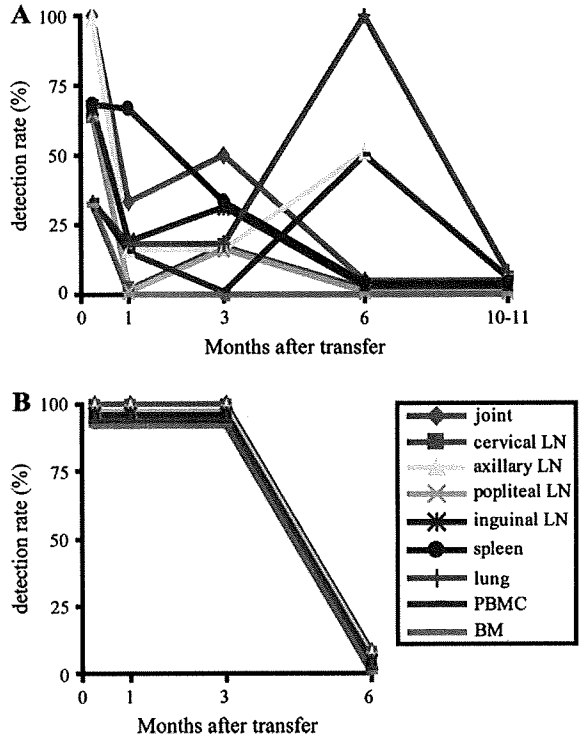

Fig. 9. Detection of TCR mRNA of the transferred clones in recipient BALB/c nude mice. 35S (A) or dengue 2F7 (B) in the recipients were detected by Southern blot analysis using primers and probes specific for TCR V and J region and CDR3 sequences of each clone. All mice with at least one positive signal out of four joints were considered to be positive. (A) $n = 3$ at 1 week; $n = 6$ at 1 month; $n = 6$ at 3 months; $n = 2$ at 6 months; $n = 2$ at 10–11 months. (B) $n = 2$ in every group. No signal was detected in control 6- or 11-month old BALB/c nude mice in each Southern blot analysis (data not shown).

histocompatible T cell-deficient mice. Furthermore, the arthritic and pulmonary lesions chronically progressed irrespective of the decline in the number of transferred T cell clones to hardly detectable levels in either lesion.

Our previous study showed that bulk $CD4^+$ T cells alone from arthritic SKG mice were able to transfer the disease to athymic nude mice, whereas bulk $CD8^+$ T cells alone were not and that abundant $CD4^+$ T cells and only a small number of $CD8^+$ T cells were found by immunohistochemistry in the arthritic subsynovial tissue of arthritic SKG mice (14). These apparently opposing results with $CD8^+$ T cell clones versus bulk $CD8^+$ T cells indicate that potentially arthritogenic $CD8^+$ T cells are present in SKG mice and may usually need $CD4^+$ T cell help for induction of arthritis; yet, they are potentially able to mediate arthritis without $CD4^+$ T cell help if they are strongly activated, clonally expanded to a large number or possibly selected for stronger self-reactivity during *in vitro* culture. It remains to be determined how $CD8^+$ clones elicit proliferative synovitis rather than cytotoxic killing of certain cellular elements in the joint. One possibility is that these $CD8^+$ clones, which exert *in vitro* killing activity at a high T cell/target cell ratio, might also be able to stimulate synoviocytes through secreting cytokines. It is of interest in this regard that the joints and the lungs with severe pneumonitis in some recipients of the $CD8^+$ clones showed active transcription of IL-17 mRNA (Supplementary Figure 1, available at *International Immunology* Online). Although the $CD8^+$ clones did not produce detectable amounts of IL-17 by *in vitro* stimulation, they might produce the cytokine in the joints or interact with nude mouse-derived α/β or γ/δ T cells and stimulate them to secrete IL-17 (33, 34). It is of note that a large number of $Gr\text{-}1^+$ mature neutrophils exuded into the joint fluid and infiltrated into the subsynovial tissue of the recipient nude mice, as in the arthritic lesions of SKG mice (14). BM of the clone recipients also showed an increase in the number of $Gr\text{-}1^+$ mature neutrophils. It remains to be determined how $CD8^+$ T cells mediate arthritis and pneumonitis in SKG mice by recruiting other cellular elements including neutrophils, how they increase neutrophils in the BM and whether IL-17, which is capable of recruiting neutrophils, is involved in these processes (35, 36).

It also needs further investigation whether IFN-γ secreted by the transferred $CD8^+$ clones or their killing activity could contribute to the development of synovitis. IFN-γ may activate synoviocytes directly or indirectly through activating macrophages, facilitating synoviocyte proliferation. It might up-regulate the expression of MHC class I in synovial cells, rendering them susceptible to cytotoxic activity of $CD8^+$ T cells. With these apparently opposing activities of arthritogenic $CD8^+$ T cells (i.e. killing versus proliferation of synoviocytes), they mediate proliferative synovitis rather than synoviocyte destruction presumably because synoviocytes might be more sensitive *in vivo* to the stimulatory effect than the cytotoxicity (see Discussion below).

The $CD8^+$ clones exhibited *in vitro* cytotoxic activity against not only syngeneic synovial cells but also a variety of MHC-matched lymphoid and non-lymphoid cell lines. Although their precise antigen specificities need to be determined, this finding suggests that these clones may recognize a ubiquitous self-antigen (for example, ubiquitous cellular protein such as hsp complexed with MHC or the MHC molecule itself) expressed in the joint and lung and other tissues, rather than a common self-antigen exclusively expressed in the joint and lung. If this is the case, how are the joint and the lung selectively affected by these T cell clones? For the following reasons, one could attribute this to unique characteristics of the synoviocytes, and possibly the alveolar macrophage, as the target of this autoimmunity. Compared with other tissue cells, the synoviocytes are

highly sensitive to pro-inflammatory cytokines, for example systemic overproduction of transgenic TNF-α or IL-1 almost exclusively produces chronic arthritis even in mice deficient of both T and B cells (37–39); similarly, systemic deficiency of the IL-1R antagonist, and resulting overproduction of IL-1, or systemic alteration of signal transduction via IL-6 receptor results in predominant development of arthritis with no inflammatory damage to other tissues (40, 41). These findings collectively indicate that synoviocytes are much more sensitive to the SKG self-reactive T cell clones (at least to those secreting pro-inflammatory cytokines) than other tissue cells, even if the common self-antigens recognized by the clones are ubiquitously expressed. In addition, synoviocytes are unique in that they are the target cells and also the mediators of autoimmunity, i.e. upon stimulation (e.g. by cytokines or via cell contact stimulation by self-reactive T cells), they proliferate and secrete pro-inflammatory cytokines (e.g. IL-1, IL-6 and TNF-α) and other inflammatory substances (matrix metalloproteinases and prostaglandins), mediating inflammation and tissue damage (42). It is likely that the cells composing the alveolar walls, in particular the alveolar macrophages, are sensitive and responsive to T cell self-reactivity in a similar manner as synoviocytes and that excessively and chronically activated macrophages might mediate alveolitis and interstitial inflammation. A similar mechanism might also be responsible for the development of colitis in SKG mice (Table 1).

We do not assert, however, that SKG arthritis and pneumonitis are solely mediated by T cells recognizing a ubiquitous common self-antigen. We have previously shown that SKG mice spontaneously produce IgG isotype auto-antibody specific for joint-rich type II collagen or IgG antibody cross-reactive with hsp-70 of Tuberculosis bacilli (14). This indicates that helper $CD4^+$ T cells that specifically react with these self-antigens may also be induced in SKG mice either primarily or secondarily to joint damage. Moreover, we have recently shown that some self-reactive T cells in SKG mice may not be arthritogenic but can polyclonally stimulate antigen-presenting cells in the spleen and lymph nodes to secrete IL-6 and other cytokines, which in turn facilitate differentiation of potentially arthritogenic self-reactive T cells to T_h17 effector T cells that mediate synovitis (19). In addition to our current approach to the characterization of antigen specificity of SKG autoimmune T cells by preparing T cell clones, efforts are being made to further characterize infiltrating T cells *in situ* at a single-cell level by amplifying their TCR message.

Tracing the fate of transferred T cell clones revealed that clone-specific TCR gene messages gradually diminished not only in the inflamed joints and the lungs but also in the regional lymph nodes and spleens of the recipients, becoming hardly detectable in 6–11 months; yet, inflammation in the joints and the lung continued to progress and severe arthritis and pneumonitis were apparent even 12 months after clone transfer. Thus, initial triggering of synovitis requires arthritogenic T cells; yet, synovitis apparently becomes less T cell dependent in a later phase, albeit it chronically progresses with the formation of pannus destroying adjacent cartilage and bone, as in human RA (2). This may correlate with the findings in humans that T cell-targeted mAb therapy is not much efficacious in the treatment of RA at a chronic stage (43). Further characterization of each stage of disease development in SKG mice will contribute to our understanding of the cellular and molecular basis of the T cell-dependent and -independent phases of disease progression in the joints and also in the lung in RA.

In conclusion, we have shown that $CD8^+$ T cell clones established from arthritogenic lesions of SKG mice are capable of mediating not only arthritis but also interstitial pneumonitis immunopathologically resembling ILD in RA. This provides a possible common pathogenetic basis between arthritis and ILD in RA. The etiology of RA is largely obscure at present (1, 2). Yet, there are recent findings that genetic polymorphism of the PTPN22-encoded lymphoid tyrosine phosphatase, which alters signal transduction at a TCR proximal step involving ZAP-70, contributes significantly (second only to MHC polymorphism) to the susceptibility to RA and other autoimmune diseases (22, 23, 44, 45). The polymorphism might be responsible for thymic generation of arthritogenic and other self-reactive T cells. Further elucidation of the mechanism by which such autoreactive T cells are generated and activated in SKG mice, and characterization of putative ubiquitous self-antigen recognized by self-reactive T cells capable of mediating arthritis and pneumonitis, would facilitate our understanding of the etiology and the pathogenetic mechanism of RA as a systemic autoimmune disease. This should help devising preventive or curative measures for the disease.

Supplementary data

Supplementary figure is available at *International Immunology* Online.

Funding

Grants-in-Aid from the Ministry of Education, Sports and Culture, the Ministry of Human Welfare of Japan; Japan Science and Technology Agency.

Acknowledgements

The authors thank Z. Fehervari for critically reading the manuscript and the members of our laboratories for valuable comments.

Disclosures

The authors declare no conflicting interests.

Abbreviations

BM	bone marrow
CDR3	the third complementarity-determining region
H&E	haematoxylin & eosin
hsp	heat shock protein
ILD	interstitial lung disease
MHA	microplate hybridization assay
PMA	phorbol myristate acetate
RA	rheumatoid arthritis
RT	reverse transcription
SSC	standard saline citrate
TNF	tumor necrosis factor
ZAP-70	ζ-associated protein of 70 kDa

References

1 Harris, E. D. 1997. *Rheumatoid Arthritis.* W.B. Sounders, Philadelphia, PA.
2 Firestein, G. S. 2003. Evolving concepts of rheumatoid arthritis. *Nature* 423:356.
3 Perez, T., Remy-Jardin, M. and Cortet, B. 1998. Airways involvement in rheumatoid arthritis: clinical, functional, and HRCT findings. *Am. J. Respir. Crit. Care Med.* 157:1658.
4 Demir, R., Bodur, H., Tokoglu, F., Olcay, I., Ucan, H. and Borman, P. 1999. High resolution computed tomography of the lungs in patients with rheumatoid arthritis. *Rheumatol. Int.* 19:19.
5 Gabbay, E., Tarala, R., Will, R. *et al.* 1997. Interstitial lung disease in recent onset rheumatoid arthritis. *Am. J. Respir. Crit. Care Med* 156:528.
6 McDonagh, J., Greaves, M., Wright, A. R., Heycock, C., Owen, J. P. and Kelly, C. 1994. High resolution computed tomography of the lungs in patients with rheumatoid arthritis and interstitial lung disease. *Br. J. Rheumatol.* 33:118.
7 Striebich, C. C., Falta, M. T., Wang, Y., Bill, J. and Kotzin, B. L. 1998. Selective accumulation of related CD4+ T cell clones in the synovial fluid of patients with rheumatoid arthritis. *J. Immunol.* 161:4428.
8 Fox, D. A. 1997. The role of T cells in the immunopathogenesis of rheumatoid arthritis: new perspectives. *Arthritis Rheum.* 40:598.
9 Panayi, G. S., Lanchbury, J. S. and Kingsley, G. H. 1992. The importance of the T cell in initiating and maintaining the chronic synovitis of rheumatoid arthritis. *Arthritis Rheum.* 35:729.
10 Nepom, G. T., Hansen, J. A. and Nepom, B. S. 1987. The molecular basis for HLA class II associations with rheumatoid arthritis. *J. Clin. Immunol.* 7:1.
11 Gao, X. J., Olsen, N. J., Pincus, T. and Stastny, P. 1990. HLA-DR alleles with naturally occurring amino acid substitutions and risk for development of rheumatoid arthritis. *Arthritis Rheum.* 33:939.
12 Firestein, G. S. and Zvaifler, N. J. 2002. How important are T cells in chronic rheumatoid synovitis? II. T cell-independent mechanisms from beginning to end. *Arthritis Rheum.* 46:298.
13 Sakaguchi, S. and Sakaguchi, N. 2005. Animal models of arthritis caused by systemic alteration of the immune system. *Curr. Opin. Immunol.* 17:589.
14 Sakaguchi, N., Takahashi, T., Hata, H. *et al.* 2003. Altered thymic T-cell selection due to a mutation of the ZAP-70 gene causes autoimmune arthritis in mice. *Nature* 426:454.
15 Hata, H., Sakaguchi, N., Yoshitomi, H. *et al.* 2004. Distinct contribution of IL-6, TNF-alpha, IL-1, and IL-10 to T cell-mediated spontaneous autoimmune arthritis in mice. *J. Clin. Invest.* 114:582.
16 Yoshitomi, H., Sakaguchi, N., Kobayashi, K. *et al.* 2005. A role for fungal {beta}-glucans and their receptor Dectin-1 in the induction of autoimmune arthritis in genetically susceptible mice. *J. Exp. Med.* 201:949.
17 Chan, A. C., Iwashima, M., Turck, C. W. and Weiss, A. 1992. ZAP-70: a 70 kd protein-tyrosine kinase that associates with the TCR zeta chain. *Cell* 71:649.
18 Negishi, I., Motoyama, N., Nakayama, K. *et al.* 1995. Essential role for ZAP-70 in both positive and negative selection of thymocytes. *Nature* 376:435.
19 Hirota, K., Hashimoto, M., Yoshitomi, H. *et al.* 2007. T cell self-reactivity forms a cytokine milieu for spontaneous development of IL-17+ Th cells that cause autoimmune arthritis. *J. Exp. Med.* 204:41.
20 Maini, R. N. and Feldmann, M. 2002. How does infliximab work in rheumatoid arthritis. *Arthritis Res.* 4:(Suppl. 2). S22.
21 Nishimoto, N., Yoshizaki, K., Miyasaka, N. *et al.* 2004. Treatment of rheumatoid arthritis with humanized anti-interleukin-6 receptor antibody: a multicenter, double-blind, placebo-controlled trial. *Arthritis Rheum.* 50:1761.
22 Bottini, N., Vang, T., Cucca, F. and Mustelin, T. 2006. Role of PTPN22 in type 1 diabetes and other autoimmune diseases. *Semin. Immunol.* 18:207.
23 Begovich, A. B., Carlton, V. E., Honigberg, L. A. *et al.* 2004. A missense single-nucleotide polymorphism in a gene encoding a protein tyrosine phosphatase (PTPN22) is associated with rheumatoid arthritis. *Am. J. Hum. Genet.* 75:330.
24 Yoshida, R., Yoshioka, T., Yamane, S. *et al.* 2000. A new method for quantitative analysis of the mouse T-cell receptor V region repertoires: comparison of repertoires among strains. *Immunogenetics* 52:35.
25 Hori, S., Nomura, T. and Sakaguchi, S. 2003. Control of regulatory T cell development by the transcription factor Foxp3. *Science* 299:1057.
26 Arden, B., Clark, S. P., Kabelitz, D. and Mak, T. W. 1995. Mouse T-cell receptor variable gene segment families. *Immunogenetics* 42:501.
27 Koop, B. F., Rowen, L., Wang, K. *et al.* 1994. The human T-cell receptor TCRAC/TCRDC (C alpha/C delta) region: organization, sequence, and evolution of 97.6 kb of DNA. *Genomics* 19:478.
28 Malissen, M., Minard, K., Mjolsness, S. *et al.* 1984. Mouse T cell antigen receptor: structure and organization of constant and joining gene segments encoding the beta polypeptide. *Cell* 37:1101.
29 Gascoigne, N. R., Chien, Y., Becker, D. M., Kavaler, J. and Davis, M. M. 1984. Genomic organization and sequence of T-cell receptor beta-chain constant- and joining-region genes. *Nature* 310:387.
30 MacDonald, H. R., Lees, R. K., Sordat, B., Zaech, P., Maryanski, J. L. and Bron, C. 1981. Age-associated increase in expression of the T cell surface markers Thy-1, Lyt-1, and Lyt-2 in congenitally athymic (nu/nu) mice: analysis by flow microfluorometry. *J. Immunol.* 126:865.
31 MacDonald, H. R., Lees, R. K., Bron, C., Sordat, B. and Miescher, G. 1987. T cell antigen receptor expression in athymic (nu/nu) mice. Evidence for an oligoclonal beta chain repertoire. *J. Exp. Med.* 166:195.
32 Hodes, R. J., Sharrow, S. O. and Solomon, A. 1989. Failure of T cell receptor V beta negative selection in an athymic environment. *Science* 246:1041.
33 He, D., Wu, L., Kim, H. K., Li, H., Elmets, C. A. and Xu, H. 2006. CD8+ IL-17-producing T cells are important in effector functions for the elicitation of contact hypersensitivity responses. *J. Immunol.* 177:6852.
34 Ivanov, I. I., McKenzie, B. S., Zhou, L. *et al.* 2006. The orphan nuclear receptor RORgammat directs the differentiation program of proinflammatory IL-17+ T helper cells. *Cell* 126:1121.
35 Edwards, S. W. and Hallett, M. B. 1997. Seeing the wood for the trees: the forgotten role of neutrophils in rheumatoid arthritis. *Immunol. Today* 18:320.
36 Jimenez-Boj, E., Redlich, K., Turk, B. *et al.* 2005. Interaction between synovial inflammatory tissue and bone marrow in rheumatoid arthritis. *J. Immunol.* 175:2579.
37 Keffer, J., Probert, L., Cazlaris, H. *et al.* 1991. Transgenic mice expressing human tumour necrosis factor: a predictive genetic model of arthritis. *EMBO J.* 10:4025.
38 Aidinis, V., Plows, D., Haralambous, S. *et al.* 2003. Functional analysis of an arthritogenic synovial fibroblast. *Arthritis Res. Ther.* 5:R140.
39 Niki, Y., Yamada, H., Seki, S. *et al.* 2001. Macrophage- and neutrophil-dominant arthritis in human IL-1 alpha transgenic mice. *J. Clin. Invest.* 107:1127.
40 Horai, R., Saijo, S., Tanioka, H. *et al.* 2000. Development of chronic inflammatory arthropathy resembling rheumatoid arthritis in interleukin 1 receptor antagonist-deficient mice. *J. Exp. Med.* 191:313.
41 Atsumi, T., Ishihara, K., Kamimura, D. *et al.* 2002. A point mutation of Tyr-759 in interleukin 6 family cytokine receptor subunit gp130 causes autoimmune arthritis. *J. Exp. Med.* 196:979.
42 Huber, L. C., Distler, O., Tarner, I., Gay, R. E., Gay, S. and Pap, T. 2006. Synovial fibroblasts: key players in rheumatoid arthritis. *Rheumatology (Oxford)* 45:669.
43 Strand, V., Kimberly, R. and Isaacs, J. D. 2007. Biologic therapies in rheumatology: lessons learned, future directions. *Nat. Rev. Drug Discov.* 6:75.
44 Vang, T., Congia, M., Macis, M. D. *et al.* 2005. Autoimmune-associated lymphoid tyrosine phosphatase is a gain-of-function variant. *Nat. Genet.* 37:1317.
45 Wu, J., Katrekar, A., Honigberg, L. A. *et al.* 2006. Identification of substrates of human protein-tyrosine phosphatase PTPN22. *J. Biol. Chem.* 281:11002.

J Pharmacol Sci 111, 338 – 351 (2009)

Journal of Pharmacological Sciences

Full Paper

Differential Coupling of Human Endothelin Type A Receptor to $G_{q/11}$ and G_{12} Proteins: the Functional Significance of Receptor Expression Level in Generating Multiple Receptor Signaling

Takahiro Horinouchi[1], Hiroshi Asano[1], Tunaki Higa[1], Arata Nishimoto[1], Tadashi Nishiya[1], Ikunobu Muramatsu[2], and Soichi Miwa[1,*]

[1]*Department of Cellular Pharmacology, Hokkaido University Graduate School of Medicine, Sapporo 060-8638, Japan*
[2]*Division of Pharmacology, Department of Biochemistry and Bioinformative Sciences, School of Medicine, University of Fukui, Fukui 910-1193, Japan*

Received August 21, 2009; Accepted September 28, 2009

Abstract. This study examines the influence of receptor expression level on signaling pathways activated via endothelin type A receptor (ET_AR) expressed in Chinese hamster ovary cells at 32,100 (ET_AR-high-CHO) and 893 (ET_AR-low-CHO) fmol·mg protein^{-1}. Endothelin-1 (ET-1) elicited a sustained increase in intracellular Ca^{2+} concentration ($[Ca^{2+}]_i$), which was dependent on $G_{q/11}$ protein, phospholipase C (PLC), Na^+/H^+ exchanger (NHE), and p38 mitogen–activated protein kinase (p38MAPK) in ET_AR-high-CHO, whereas the sustained $[Ca^{2+}]_i$ increase was negligible in ET_AR-low-CHO. Functional study with Cytosensor™ microphysiometer showed that ET-1 evoked an NHE1-mediated increase in extracellular acidification rate (ECAR) in ET_AR-high-CHO and ET_AR-low-CHO. In ET_AR-high-CHO, the ECAR response at 30 min after ET-1 stimulation was insensitive to $G_{q/11}$ and PLC inhibitors, but sensitive to the p38MAPK inhibitor. In ET_AR-low-CHO, the ECAR response at 30 min was sensitive to these inhibitors. Western blot analysis demonstrated that ET-1–induced p38MAPK phosphorylation in ET_AR-low-CHO but not in ET_AR-high-CHO was mediated via $G_{q/11}$ and PLC. The $G_{q/11}$/PLC-independent p38MAPK phosphorylation in ET_AR-high-CHO was suppressed by expression of the C terminus of $G_{\alpha 12}$ protein to disrupt receptor-G_{12} protein coupling. These results provide evidence for multiple signaling pathways of ET_AR that were activated via at least the $G_{q/11}$/PLC/NHE, G_{12}/p38MAPK/NHE, and $G_{q/11}$/PLC/p38MAPK/NHE cascades in an expression level–dependent manner.

Keywords: endothelin type A receptor, receptor expression level, intracellular free Ca^{2+} concentration, Na^+/H^+ exchanger, p38 mitogen–activated protein kinase

Introduction

Endothelin type A receptor (ET_AR) belongs to the superfamily of G protein-coupled receptors (GPCRs) that transduce the binding of their agonists into activation of G protein–regulated effectors and elevation of the corresponding second messengers. It is generally accepted that human ET_AR can couple with several subfamilies of a heterotrimeric G protein family including G_q, G_s, and G_{12}. Typically, G_q protein activated by stimulation of ET_AR with its agonist, endothelin-1 (ET-1), induces formation of second messengers such as inositol 1,4,5-trisphosphate (IP_3) and diacylglycerol (DAG) via phospholipase Cβ (PLCβ); G_s induces formation of cyclic AMP (cAMP) via adenylyl cyclase (AC); G_{12} induces formation of actin stress fiber via a Rho/ROCK system (1, 2).

Ca^{2+} signal plays a key role in controlling diverse cellular functions such as contraction, proliferation, and transcription. Activation of endogenous ET_AR in vascular smooth muscle cells and recombinant ET_AR expressed in Chinese hamster ovary (CHO) cells evokes

*Corresponding author. smiwa@med.hokudai.ac.jp
Published online in J-STAGE on November 27, 2009 (in advance)
doi: 10.1254/jphs.09233FP

an increase in intracellular free Ca^{2+} concentration ($[Ca^{2+}]_i$) that consists of the following two phases: an initial transient increase and a subsequent sustained increase (1, 3 – 6). Pharmacological and electrophysiological studies using $[Ca^{2+}]_i$ measurement and whole-cell patch clamp have shown that the transient $[Ca^{2+}]_i$ increase is due to IP_3-mediated Ca^{2+} release from endoplasmic reticulum, whereas the ET-1–induced sustained $[Ca^{2+}]_i$ increase is due to Ca^{2+} influx through voltage-independent, Ca^{2+}-permeable nonselective cation channel (NSCC), which is a member of the receptor-operated Ca^{2+} channels (ROCCs) (1, 2, 4, 5), and Na^+/Ca^{2+} exchanger (NCX) operated via Na^+ influx resulting from activation of Na^+/H^+ exchanger (NHE) (7). Among G_q, G_s, and G_{12} proteins coupled with ET_AR, G_q, and G_{12} are reported to be involved in activation of NSCCs triggered by ET-1 in CHO cells expressing recombinant human ET_AR (1, 2). In contrast, ET_AR signaling cascades required for activation of NHE regulating extracellular acidification rate (ECAR) are less well characterized.

Recently, accumulating evidence from a variety of GPCRs such as calcitonin, opioid, and β-adrenergic receptors (β-ARs) has demonstrated that an agonist activating the same receptor can trigger pleiotropic effects, although the same cellular response pattern with or without differences in their potency and/or efficacy has been assumed on the basis of traditional pharmacological concepts (8 – 10). This phenomenon has been referred to by many names including "ligand-directed signaling", "agonist-directed trafficking", "biased agonism", "protean agonism", or "functional selectivity" (8, 9, 11, 12). One of the important factors giving such multiple signaling generated by stimulation of a single GPCR is the receptor expression level that affects receptor–G protein coupling in recombinant expression systems (9, 10). For example, stimulation of G_s-coupled calcitonin receptors expressed in human embryonic kidney (HEK) 293 cells at low level causes cAMP production, whereas higher level of receptor expression leads to an increase in $[Ca^{2+}]_i$ in addition to cAMP, implying that $G_{q/11}$ coupling to calcitonin receptors is dependent on their expression levels (10). Thus, excessive expression of GPCRs results in production of multiple coupling of the receptors to various G proteins, possibly due to loss of the fidelity of receptor–G protein coupling (13). It remains to be determined how the expression level of recombinant human ET_AR influences coupling of the receptors with G proteins and its downstream-signaling, although the receptor–G protein coupling depending on the receptor density can control not only the quantity of the GPCR-mediated response but also the quality of the response.

The present study examined receptor density–linked activation of signaling pathways in order to explore the multiple signaling pathways of human ET_AR. The results with CHO cells expressing ET_AR at different expression levels provide evidence that coupling of ET_AR to $G_{q/11}$ and G_{12} varies depending on the expression levels of the receptors, leading to the activation of different signaling cascades for the human ET_AR. The lack of ET_AR-G_{12} coupling results in the disappearance of sustained Ca^{2+} influx. ET_AR can utilize multiple signaling pathways including $G_{q/11}$/PLC/NHE, G_{12}/p38 mitogen–activated protein kinase (p38MAPK)/NHE, and $G_{q/11}$/PLC /p38MAPK/NHE cascades to induce the same functional response, an increase in ECAR.

Materials and Methods

Materials

YM-254890 was kindly provided by Astellas Pharma, Inc. (Tokyo). The following drugs and regents were used in the present study: synthetic human ET-1 (Peptide Institute, Osaka); fura-2/acetoxymethyl ester (fura-2 /AM), fluo-3/AM, Pluronic F-127 (Dojindo Laboratories, Kumamoto); SB203580 hydrochloride [4-(4-fluorophenyl)-2-(4-methylsulfinyl phenyl)-5-(4-pyridyl) 1*H*-imidazole hydrochloride], 2',5'-dideoxyadenosine, NF449 {4,4',4",4"'-[carbonyl-bis[imino-5,1,3-benzene-triylbis-(carbonylimino)]]tetrakis-(benzene-1,3-disulfonate}, U-73122 {1-[6-((17β-3-methoxyestra-1,3,5(10)-trien-17-yl)amino)hexyl]-1*H*-pyrrole-2,5-dione} (Calbiochem, San Diego, CA, USA); PD142893 (*N*-acetyl-β-phenyl-D-Phe-Leu-Asp-Ile-Ile-Trp), EIPA [5-(*N*-ethyl-*N*-isopropyl)amiloride], probenecid, aprotinin, leupeptin, pepstatin, sodium deoxycholate, sodium dodecyl sulfate (SDS), phenylmethylsulfonyl fluoride (PMSF), Na_3VO_4, NaF, puromycin dihydrochloride (Sigma-Aldrich Co., St. Louis, MO, USA); [^{3}H]BQ123 {cyclo-(D-Trp-D-Asp-[prolyl-3,4(*n*)-^{3}H]-D-Val-Leu), specific activity: 18.0 Ci/mmol} (Amersham Biosciences, Amersham Place Little Chalfont, Buckinghamshire, UK). All cell culture media and supplements except fetal calf serum (FCS; Invitrogen Corp., Grand Island, NY, USA) were obtained from Sigma-Aldrich. Antibodies were obtained from Cell Signaling Technology, Inc. (Beverly, MA, USA). The other regents used were of the highest grade in purity.

Cell culture

CHO cells were grown as monolayers cultured in Ham's F-12 medium supplemented with 10% ($v \cdot v^{-1}$) FCS, penicillin (100 units $\cdot$ ml^{-1}), and streptomycin (100 μg $\cdot$ ml^{-1}) at 37°C in humidified air with 5% CO_2.

Stable expression of human ET_AR in CHO cells

The gene of human ET_AR fused with yellow fluorescence protein (YFP) at the C terminus was introduced into CHO cells by retroviral gene transfer as previously described (6). The cells were grown for 48 h and then stable transformants were selected in medium containing 5 $\mu g \cdot ml^{-1}$ puromycin for a week. The cells were sorted into eight populations by using flow cytometry (FACSVantage™; BD Biosciences, San Jose, CA, USA) based on their YFP fluorescence intensity. Clonal cell lines were obtained by limiting dilution of each cell population. Clones were expanded and screened for expression levels by radioligand binding analyses with a single concentration of [^{3}H]BQ-123 (2 nM). Suitable clones were grown up for a full saturation binding assay.

Whole-cell binding assay

Saturation binding assay was conducted with intact cells using the radioligand [^{3}H]BQ-123. CHO cells expressing human ET_AR at different expression level were washed twice and harvested with 0.02% EDTA in phosphate-buffered saline (PBS; pH 7.4) by gentle pipetting. The resulting cell pellets were washed once and resuspended in Ca^{2+}-free Krebs-HEPES solution (140 mM NaCl, 3 mM KCl, 1 mM $MgCl_2 \cdot 6H_2O$, 11 mM D-(+)-glucose, 10 mM HEPES; adjusted to pH 7.3 with NaOH) at $1 - 5 \times 10^6$ cells/ml. Intact cells were incubated in 500 μl of Ca^{2+}-free Krebs-HEPES solution containing 0.1% bovine serum albumin (BSA) with [^{3}H]BQ-123 at concentrations ranging 0.1 – 5 nM at 4°C for 24 h. To avoid radioligand depletion, cell number in each incubation tube was adjusted to $0.5 - 2.5 \times 10^5$ cells, depending on their receptor expression levels. Nonspecific binding was defined by the presence of 1 μM PD142893, a nonselective ET_AR and ET_BR antagonist (14). Assays were terminated by rapid filtration using a Brandel cell harvester (Brandel, Inc., Gaithersburg, MD, USA) over Whatman GF/C filters presoaked with 0.3% polyethyleneimine for 60 min. The filters were rapidly washed 3× with 5-ml aliquots of ice-cold washing buffer (50 mM Tris-HCl, pH 7.4), and dried before the measurement of filter-bound radioactivity. The radioactivity was counted in a liquid scintillation counter (LC-3500; Aloka, Tokyo) using a scintillation fluid (Clear-sol II; Nacalai Tesque, Kyoto). The protein contents were determined by the method of Bradford (15) using BSA as standard.

Measurement of ECAR

The eight-channel Cytosensor™ microphysiometer (Molecular Devices Corp., Sunnyvale, CA, USA) was used to measure ET_AR-mediated changes in ECAR. Briefly, CHO cells expressing ET_AR were seeded into 12-mm capsule cups at density of 5×10^5 cells per cup and cultured in Ham's F-12 medium supplemented with 0.5% FCS at 37°C in an atmosphere of 5% CO_2 for 24 h. On the day of the experiment, the capsule cups were loaded into the sensor chambers of the instrument, and the chambers were perfused with running medium, which was modified RPMI-1640 (Molecular Devices Corp.) containing 0.1% BSA, at a flow rate of 100 $\mu l \cdot min^{-1}$. During a 2-min pump cycle, the pump was on for 1 min 20 s and then switched off for the remaining 40 s. The ECAR was measured from 1:28 to 1:58 min in every cycle. The paired sister cells were equilibrated for 90 min and then were treated with either vehicle [0.2% dimethylsulfoxide (DMSO)] or inhibitors for 30 min before stimulation with ET-1 for 30 min. Final DMSO concentration in the medium did not affect the ECAR responses to ET-1 (data not shown). All drugs were diluted into running medium and perfused through either fluid path. Results are expressed as a % of the basal ECAR prior to exposure to DMSO or inhibitor.

Adenovirus infection

Recombinant adenoviruses encoding green fluorescence protein (GFP) and the C-terminus region of $G_{\alpha 12}$ protein ($G_{\alpha 12}$-ct) along with GFP protein (16) were kindly provided by Dr. Hitoshi Kurose (Kyushu University, Fukuoka). CHO cells grown to 100% confluence in six-well plates at a density of approximately 3×10^6 cells/well were infected by recombinant adenovirus for 2 h at 300 multiplicity of infection (MOI). After infection, the cells were cultured in Ham's F-12 medium containing 0.5% FCS for 60 h. Subsequently, the cells were maintained for 12 h in the absence of FCS for Western blot analysis. To estimate the efficiency of adenoviral infection in CHO cells, expression level of recombinant protein GFP was determined by flow cytometry analysis.

Flow cytometry analysis

CHO cells with or without adenovirus infection grown in six-well plates were harvested with 0.02% EDTA in PBS and then resuspended in PBS containing 1% FCS and 0.01% NaN_3. The cell suspensions were analyzed on a FACSCalibur™ flow cytometer (BD Biosciences) using CellQuest software (BD Biosciences).

Detection of mRNA for $G_{\alpha 12}$-ct by reverse transcription–polymerase chain reaction (RT-PCR)

Total RNA was isolated from CHO cells infected by recombinant adenovirus encoding GFP or $G_{\alpha 12}$-ct along with GFP using an RNeasy Kit (QIAGEN K.K., Tokyo) according to the manufacturer's protocol. The isolated RNA was reverse transcribed using the SuperScript™

First-Strand Synthesis System Kit (Invitrogen), and the resultant first-strand cDNA was applied to PCR, which was performed using a HotStarTaq™ Master Mix Kit (QIAGEN K.K.). A negative control without reverse transcriptase was run in parallel to verify that amplification did not proceed from residual genomic DNA. The sequences of the forward and reverse primers were 5'-GATCCGCTAGAGATCTGGTACCATG-3' and 5'-CTGCAGCATGATGTCTTTCAGGTTC-3', respectively (16). cDNA was heated for 15 min at 95°C and then amplified by 35 cycles (95°C for 30 s, 55°C for 30 s, 72°C for 30 s) followed by 5 min of extension at 72°C. The PCR products were confirmed by a single band on electrophoresis with 2.0% ethidium bromide–stained agarose gels.

Measurement of $[Ca^{2+}]_i$

$[Ca^{2+}]_i$ was monitored by using a fluorescent Ca^{2+} indicator, fura-2/AM, as described previously (6, 17). In the experiments using SB203580 and EIPA, $[Ca^{2+}]_i$ was measured using fluo-3 (excitation = 490 nm, emission = 540 nm) instead of fura-2, because addition of these inhibitors was found to interfere with fluorescence signals of fura-2 (data not shown).

Western blot analysis

Cells grown in six-well plates were serum-starved for 12 h before drug treatment. After the various treatments, cells were washed with ice-cold PBS, and collected into lysis buffer (150 mM NaCl, 1.5 mM $MgCl_2$, 50 mM Tris-HCl (pH 6.8), 1% NP-40, 0.5% sodium deoxycholate, 0.1% SDS, 1 mM PMSF, 1 mM Na_3VO_4, 20 mM NaF, 10 $\mu g \cdot ml^{-1}$ leupeptin, 10 $\mu g \cdot ml^{-1}$ aprotinin, and 10 $\mu g \cdot ml^{-1}$ pepstatin) supplemented with EDTA-free, protease inhibitor cocktail (PIERCE Biotechnology, Inc., Rockford, IL, USA). The cell lysates were sonicated for 10 s and centrifuged at 15,000 rpm for 10 min at 4°C. The resulting supernatants were combined with SDS sample buffer [62.5 mM Tris-HCl (pH 6.8), 10% glycerol, 5% 2-mercaptoethanol (2-ME), 2.5% SDS, 0.1% bromphenol blue] followed by heating to 100°C for 5 min. The samples were separated on a 12.5% polyacrylamide gel (SuperSep™; Wako Pure Chemical Industries, Ltd., Osaka) and electrotransferred to a polyvinylidene fluoride membrane (Immobilon™-P, pore size 0.45 μm; Millipore Corp., Bedford, MA, USA) with a semi-dry electroblotter. After transfer, the membranes were washed with Tris-buffered saline-Tween 20 [TBST: 10 mM Tris-HCl (pH 8.0), 100 mM NaCl, and 1% Tween-20] for 5 min followed by blocking (5% non-fat dry milk in TBST) of nonspecific binding for 1 h at room temperature. The membranes were incubated with a phospho-p38MAPK (Thr180/Tyr182) antibody as a primary antibody overnight at 4°C. The primary antibody was detected with a secondary horseradish peroxidase–conjugated anti-rabbit IgG antibody and enhanced chemiluminescence (ECL, Amersham Biosciences). The membranes were then stripped with stripping buffer [62.5 mM Tris-HCl (pH 7.0), 2% SDS, 1% 2-ME] for 1 h at 50°C and reprobed with a p38MAPK antibody, detected with the same secondary antibody. The blots were exposed to Amersham Hyperfilm™ ECL (GE Healthcare Limited, Little Chalfont, Buckinghamshire, UK). Optical density on the film was analyzed with National Institutes of Health Image J1.37 software. p38MAPK phosphorylation was routinely expressed as the ratio of phosphorylated p38MAPK to total p38MAPK.

Data analyses

Data regarding ECAR and $[Ca^{2+}]_i$ were collected and analyzed by using the Cytosoft™ (Molecular Devices Corp.) and a MacLab/8s with Chart (v. 3.5) software (ADInstruments Japan, Tokyo), respectively. The concentration–response curves for ET-1 were constructed to evaluate its EC_{50} value, which is the effective ET-1 concentration (M) eliciting a half-maximal response using GraphPad PRISM™ (version 3.00; GraphPad Software, Inc., San Diego, CA, USA). The EC_{50} values were converted to negative logarithmic values (pEC_{50}) for analysis. Saturation binding data were analyzed by non-linear regression using GraphPad PRISM™. The computer software provides equilibrium dissociation constants (K_D) and maximum number of binding sites (B_{max}) from saturation curves. Abundance of ET_AR in CHO cells was represented as the binding capacity per milligram of protein for each (B_{max}: femtomoles per milligram of protein). All data are presented as means ± S.E.M. where n refers to the number of experiments. The significance of the difference between mean values was evaluated with GraphPad PRISM™ by Student's paired *t*-test, unpaired *t*-test, or one-way analysis of variance (ANOVA) followed by Tukey's multiple comparison test. A *P* value less than 0.05 was considered to indicate a significant difference.

Results

Radioligand binding experiments

Eighteen stable cell lines obtained by limiting dilution showed different expression levels of human ET_AR ranging from 32,100 ± 5,913 (ET_AR-high-CHO; n = 4, Fig. 1A) to 893 ± 66 (ET_AR-low-CHO; n = 4, Fig. 1B) fmol · mg protein^{-1} as measured with saturation binding assays. The two cell lines, designated as ET_AR-high-CHO and ET_AR-low-CHO, were used for analyzing

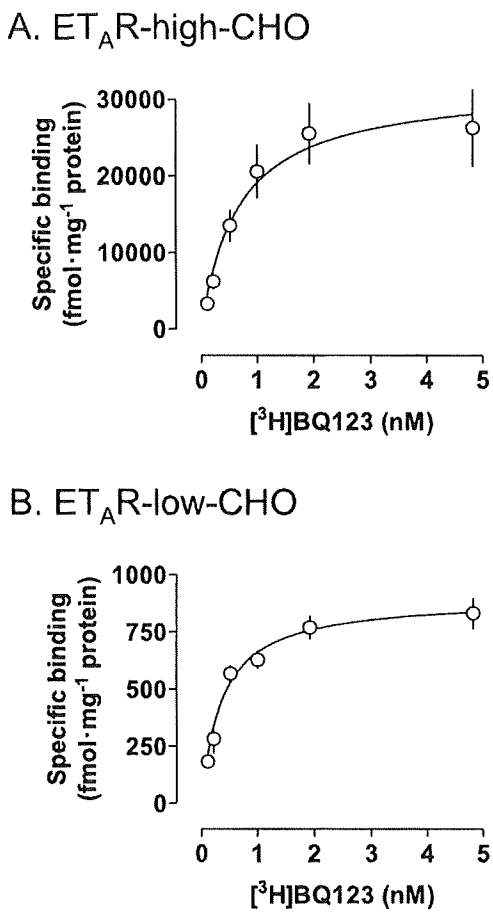

Fig. 1. Saturation binding experiments with [^{3}H]BQ123 (0.1 – 5 nM) in ET_AR-high-CHO (A) and ET_AR-low-CHO (B) using the whole-cell binding assay. Nonspecific binding was determined in the presence of PD142893 (1 μM). Each point represents the mean ± S.E.M. of 4 experiments. When no error bar is shown, the error is smaller than the symbol.

ET_AR signaling, since there was a marked difference between both cell lines in Ca^{2+} responses to ET-1, as described later. The pK_D values of ET_AR-high-CHO and ET_AR-low-CHO were 9.2 ± 0.1 (n = 4) and 9.5 ± 0.1 (n = 4), respectively. The comparable pK_D values for both groups indicated that the differences in receptor expression level had little or no effect on [^{3}H]BQ123 binding affinity for ET_AR.

Characterization of ET-1–induced increases in $[Ca^{2+}]_i$

We determined concentration–response curves for ET-1–induced increases in $[Ca^{2+}]_i$ in ET_AR-high-CHO and ET_AR-low-CHO. In wild-type CHO cells (not transfected ET_AR), ET-1 at concentrations up to 10 nM did not show any effect on $[Ca^{2+}]_i$ (data not shown), suggesting that the ET-1–induced Ca^{2+} mobilization was solely mediated by recombinant ET_AR.

In ET_AR-high-CHO, ET-1 began to induce a transient increase in $[Ca^{2+}]_i$ at 0.01 nM, which reached the maximum level at 0.3 nM, with an EC_{50} value of around 0.01 nM (Fig. 2A). Notably, the sustained increase began to appear at 0.01 nM, reached the maximum level at 0.3 nM, and remained at the similar level up to the concentration of 10 nM: the EC_{50} value was around 0.2 nM. The biphasic $[Ca^{2+}]_i$ responses consisting of transient and sustained increases were observed in other cell lines expressing ET_AR at levels over 2,700 fmol · mg protein^{-1} (Table 1). The maximum increases in $[Ca^{2+}]_i$ by ET-1 and its pEC_{50} values are summarized in Table 1.

In contrast, in ET_AR-low-CHO, ET-1 began to induce a transient increase in $[Ca^{2+}]_i$ at 0.03 nM, which was not accompanied by a sustained phase (Fig. 2B). The transient increase reached the maximum level at 3 nM, with an EC_{50} value of around 0.3 nM (Table 1). Notably, the sustained increase in $[Ca^{2+}]_i$ was very small throughout the tested concentrations of ET-1 (Fig. 2B).

The difference in sustained Ca^{2+} responses between these cell lines suggested that discrete intracellular signaling(s) is involved in development of the sustained phase triggered by ET-1, which is independent of the transient Ca^{2+} responses. To determine the influence of receptor expression levels on ET_AR signaling, subsequent experiments focused on the responses to ET-1 at 0.3 nM and 3 nM for ET_AR-high-CHO and ET_AR-low-CHO, respectively.

Determination of signaling molecules involved in the sustained increases in $[Ca^{2+}]_i$ induced by ET-1 in ET_AR-high-CHO

Stimulation of ET_AR with ET-1 is well known to elicit an increase in $[Ca^{2+}]_i$ via α-subunits derived from G_q protein (2). To confirm involvement of G_q protein in the ET-1–induced sustained increases in $[Ca^{2+}]_i$ in ET_AR-high-CHO, YM-254890, a novel $G_{\alpha q/11}$ inhibitor (18), was added during the sustained phase after stimulation of ET_AR with 0.3 nM ET-1. As shown in Fig. 3, 1 μM YM-254890 markedly inhibited the ET-1–induced sustained increases in $[Ca^{2+}]_i$, indicating that the sustained Ca^{2+} responses to ET-1 are mediated via $G_{\alpha q/11}$, as reported previously (6).

The principal downstream effector for $G_{\alpha q/11}$ is PLCβ that cleaves the membrane lipid phosphatidylinositiol-4,5-bisphosphate (PIP_2) into the second messengers such as IP_3 and DAG, both of which modulate $[Ca^{2+}]_i$ (19). In ET_AR-high-CHO, U-73122, a PLC inhibitor (6, 17), at the concentration of 3 μM significantly inhibited the ET-1–induced sustained $[Ca^{2+}]_i$ increase (Fig. 3). This result suggested that the Ca^{2+} mobilization activated by ET-1 depends on PLC activation.

An NHE-dependent mechanism is also reported to be involved in an increase in $[Ca^{2+}]_i$ triggered by stimula-

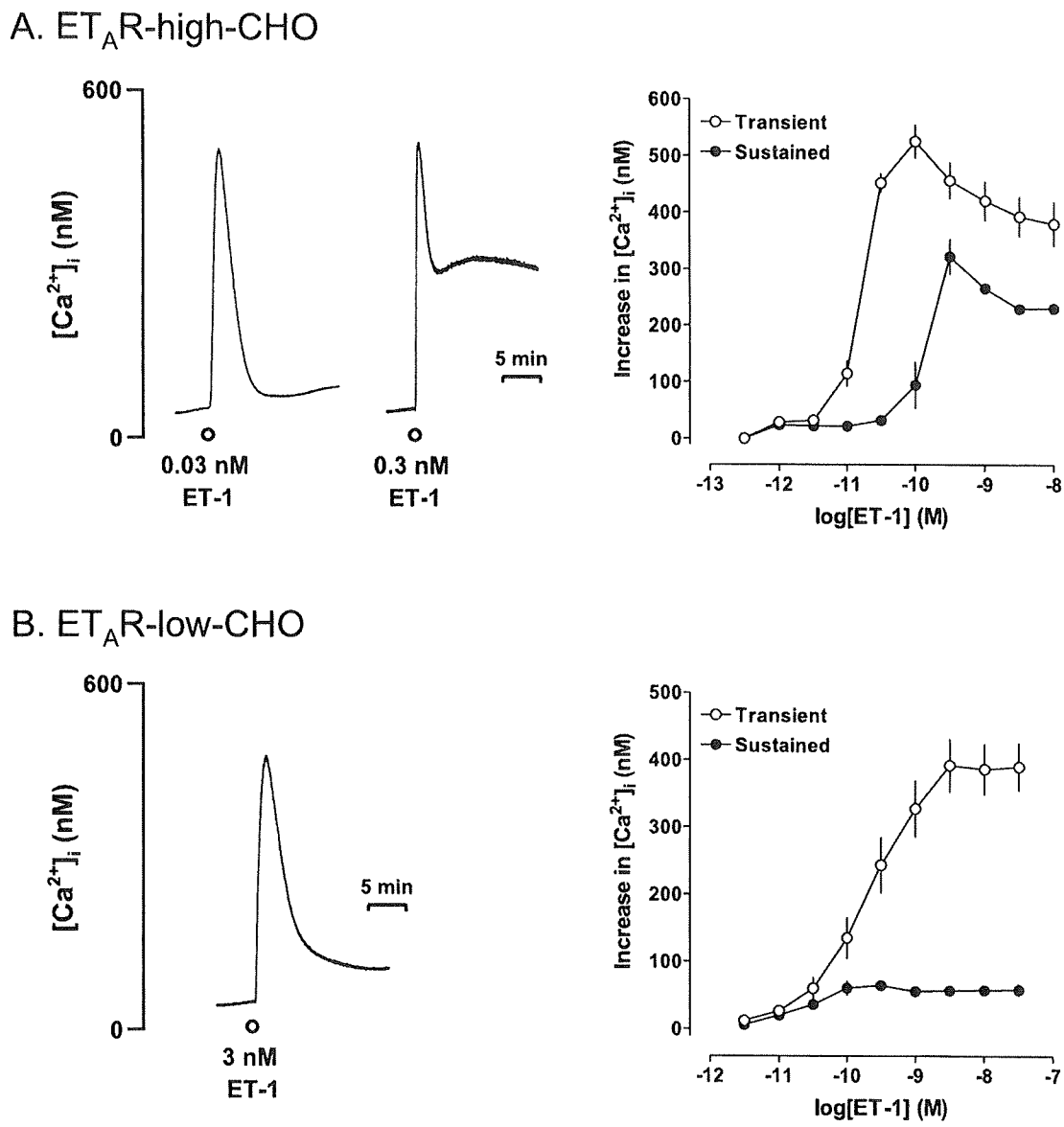

Fig. 2. Characterization of the ET-1–induced increase in $[Ca^{2+}]_i$ in ET_AR-high-CHO (A) and ET_AR-low-CHO (B). Left panels: representative traces showing the $[Ca^{2+}]_i$ increases induced by ET-1 at the indicated concentrations in ET_AR-high-CHO and ET_AR-low-CHO. Right panels: concentration–response curves for the ET-1–induced transient and sustained $[Ca^{2+}]_i$ increases. Data are presented as means ± S.E.M. of the results obtained from 5 experiments.

tion of ET_AR (7). That is, ET-1 activates NHE, causing an increase in the intracellular Na^+ concentration ($[Na^+]_i$) that in turn drives NCX operating in the reverse mode to transport Ca^{2+} into cells in exchange for Na^+ efflux, leading to an increase in $[Ca^{2+}]_i$. As indicated previously (7), pretreatment of the cells with 10 μM EIPA, a selective NHE1 inhibitor (20), partly inhibited the ET-1–induced sustained increase in $[Ca^{2+}]_i$ to 46.2 ± 2.2% (Fig. 3).

There is accumulating evidence that p38MAPK plays a functional role in ET-1–induced responses such as vascular smooth muscle contractions (21, 22). In addition, p38MAPK is a major activator of NHE (9). To clarify possible involvement of p38MAPK in Ca^{2+} responses to ET-1 in ET_AR-high-CHO, the effect of SB203580, a p38MAPK inhibitor, was examined. SB203580 inhibited the sustained increases in $[Ca^{2+}]_i$ elicited by ET-1 in a concentration-dependent manner (Fig. 3), indicating that p38MAPK also contributes to generation of the sustained Ca^{2+} influx.

Functional analysis of ET_AR signaling involved in ECAR response to ET-1 using Cytosensor™

To further analyze signaling pathways activated by

Table 1. Comparison of potencies for ET-1 on human ET_AR expressed at different levels in CHO cells estimated by $[Ca^{2+}]_i$ measurements

Expression level (fmol·mg protein^{-1})	n	Transient phase		Sustained phase	
		pEC_{50}	$[Ca^{2+}]_{iMAX}$ (nM)	pEC_{50}	$[Ca^{2+}]_{iMAX}$ (nM)
32,100 (ET_AR-high-CHO)	5	10.89 ± 0.05	525.7 ± 28.6	10.05 ± 0.09	321.9 ± 30.5
4,532	5	10.48 ± 0.01	506.4 ± 25.9	9.47 ± 0.09	289.8 ± 16.9
2,700	4	10.51 ± 0.03	639.2 ± 30.9	9.31 ± 0.03	359.6 ± 19.9
893 (ET_AR-low-CHO)	5	9.57 ± 0.03	391.7 ± 39.2	Not determined[a]	64.5 ± 5.5[a]

Results are presented as means ± S.E.M. of n number of experiments. The pEC_{50} value is the negative logarithm of the effective ET-1 concentration (M) that produces a 50% response of the maximum response, $[Ca^{2+}]_{iMAX}$. [a]Residual component of $[Ca^{2+}]_i$ after transient increase in $[Ca^{2+}]_i$ induced by ET-1, since a significant sustained phase was not generated in ET_AR-low-CHO.

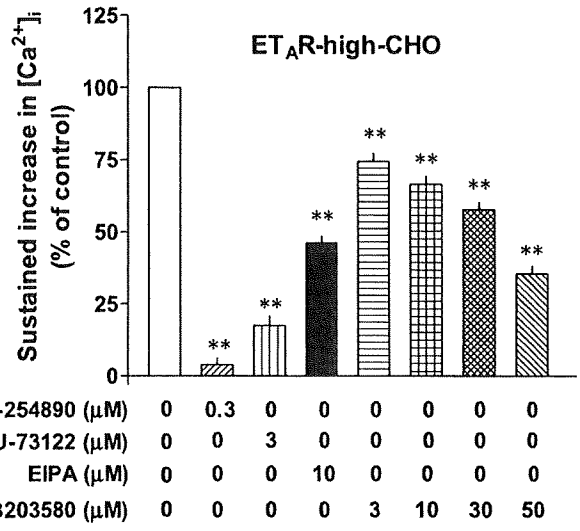

Fig. 3. Effects of YM-254890, U-73122, EIPA, and SB203580 on the sustained increases in $[Ca^{2+}]_i$ induced by 0.3 nM ET-1 in ET_AR-high-CHO. These inhibitors were added during the sustained phase after stimulation with ET-1. The $[Ca^{2+}]_i$ level induced by 0.3 nM ET-1 before addition of the inhibitors was set to 100% as a control. Data are presented as means ± S.E.M. of the results obtained from 4 – 6 experiments. $^{**}P<0.01$, vs. its control (0.3 nM ET-1 alone, open column).

ET_AR, the change in ECAR was continuously measured every 2 min by using the Cytosensor™ microphysiometer that allows the analysis of signaling molecules activated by GPCRs in living cells (23).

In ET_AR-high-CHO, 0.3 nM ET-1 induced an increase in ECAR (Fig. 4A). The ECAR response to ET-1 was completely inhibited by 10 μM EIPA, indicating the predominant role of NHE1 in the ECAR responses. To elucidate upstream signaling cascades in activation of NHE1, the effects of YM-254890, U-73122, and SB203580 on the increase in ECAR response to ET-1 were examined. Surprisingly, the sensitivity of the ECAR response to these inhibitors changed appreciably with time in ET_AR-high-CHO (Fig. 4A). Unlike the Ca^{2+} response to ET-1, the early ECAR response to ET-1 (e.g., at 2 min after ET-1 stimulation) was sensitive to either 1 μM YM-254890 or 10 μM U-73122, but insensitive to 50 μM SB203580. In contrast, the late ECAR response (e.g., at 30 min) was resistant to both YM-254890 and U-73122, whereas it was sensitive to SB203580 (Fig. 4A). These findings raised the interesting possibility that a major contributor to the ET-1–induced ECAR response in ET_AR-high-CHO varies with time from the $G_{\alpha q/11}$/PLC-dependent, p38MAPK-independent pathway to the $G_{\alpha q/11}$/PLC-independent, p38MAPK-dependent pathway.

In contrast to ET_AR-high-CHO, the increases in ECAR induced by ET-1 in ET_AR-low-CHO were sensitive to all inhibitors mentioned above until 30 min after ET-1 addition (Fig. 4B), implying the involvement of $G_{\alpha q/11}$, PLC, and p38MAPK in the ECAR response to ET-1.

It is reported that ET_AR is able to couple with G_s protein in addition to G_q and G_{12} proteins (1, 2). Activation of AC by stimulation of G_s protein–coupled β_3-ARs is reported to result in an increase in ECAR (9). However, possible involvement of the G_s/AC pathway in the ET_AR-mediated ECAR response can be ruled out, since NF449 (100 μM), a G_s inhibitor (24), and 2',5'-dideoxyadenosine (50 μM), an AC inhibitor (9), had no inhibitory effect on the ET-1–induced change in ECAR in ET_AR-high-CHO and ET_AR-low-CHO (data not shown).

Characterization of ET-1–induced phosphorylation of p38 MAPK

To confirm the involvement of p38MAPK in the ET_AR signaling, phosphorylation levels of p38MAPK was estimated by Western blot analysis. ET-1 at concentrations of 0.3 and 3 nM induced phosphorylation of p38MAPK in ET_AR-high-CHO and ET_AR-low-CHO, respectively, and the maximum phosphorylation responses were maintained up to 10 min (Fig. 5A). Treatment of both cell lines with ET-1 elicited phosphorylation of p38MAPK in a concentration-dependent manner with pEC_{50} values of 10.16 ± 0.21 and 9.64 ±

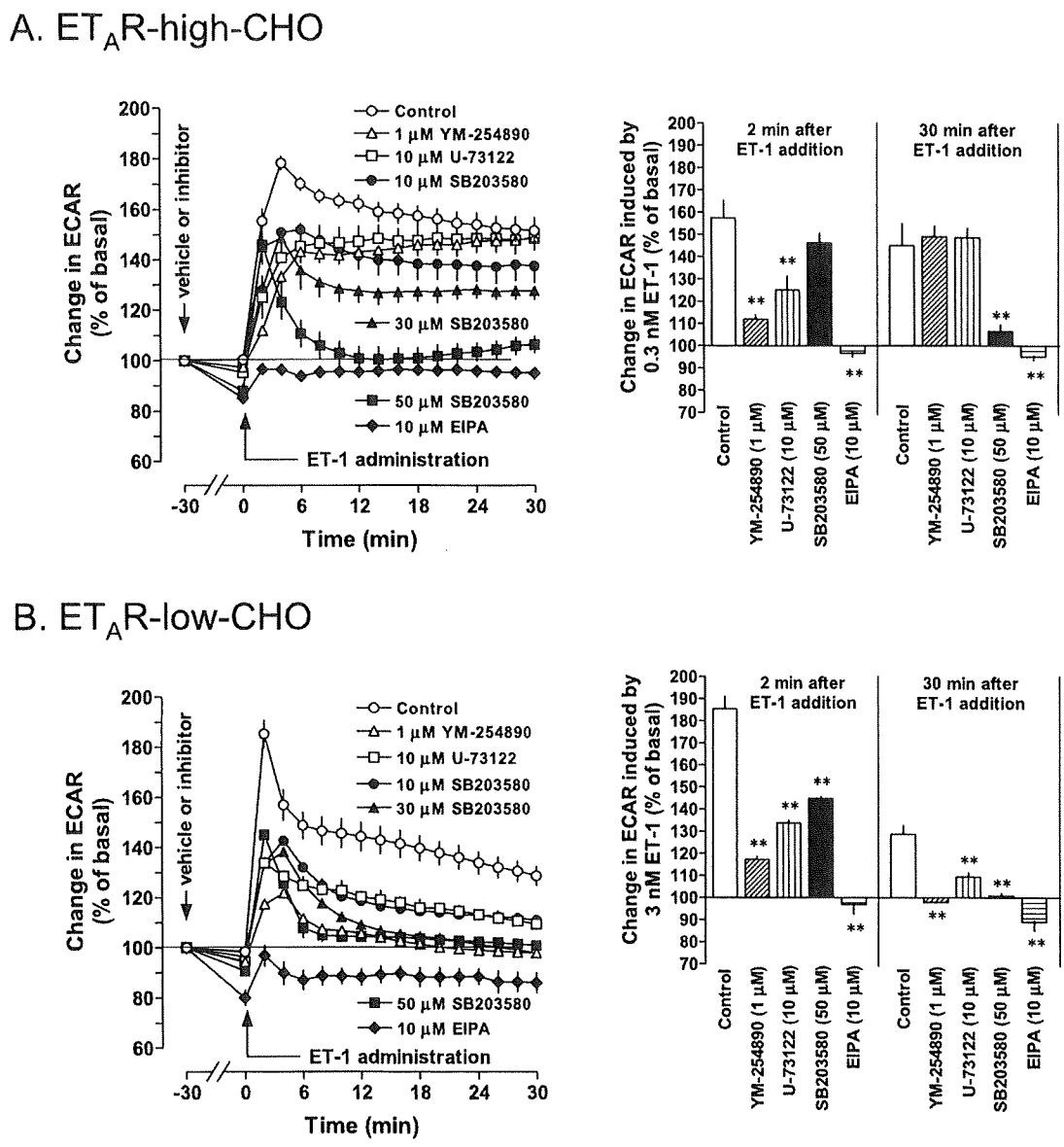

Fig. 4. Characterization of changes in ECAR induced by 0.3 nM ET-1 in ET_AR-high-CHO (A) and by 3 nM ET-1 in ET_AR-low-CHO (B). The change in ECAR was measured by the Cytosensor™ microphysiometer every 2 min. The cells were treated with either vehicle (0.2% DMSO) or inhibitor for 30 min before stimulation with ET-1 (ET-1 administration) for 30 min. Effects of YM-254890, U-73122, SB203580, and EIPA on the ECAR response to ET-1 at 2 and 10 min are shown in the right panel. Data are presented as means ± S.E.M. of the results obtained from 4 – 6 experiments. $^{**}P<0.01$, vs. its control (ET-1 alone, open column).

0.23, respectively, which reached the maximum levels of 971.6 ± 50.8% and 591.3 ± 80.7%, respectively (Fig. 5B).

To determine upstream regulatory molecules for p38MAPK, the effects of inhibitors for $G_{\alpha q/11}$ and PLC on the ET-1–induced phosphorylation of p38MAPK were examined. YM-254890 (1 μM) had little or no effect on the p38MAPK phosphorylation by ET-1 in ET_AR-high-CHO (Fig. 6A), whereas it significantly inhibited the phosphorylation in ET_AR-low-CHO (Fig. 6B). U-73122 (10 μM) itself increased phosphorylation of p38MAPK. In the presence of U-73122 (10 μM), ET-1 still caused phosphorylation of p38MAPK in ET_AR-high-CHO (Fig. 6A). In contrast, ET-1 failed to induce a further increase in p38MAPK phosphorylation in ET_AR-low-CHO treated with U-73122 (Fig. 6B). These results suggested that activation of p38MAPK after ET-1 treatment was predominantly mediated via the non-$G_{\alpha q/11}$/PLC pathway in ET_AR-high-CHO but the $G_{\alpha q/11}$/PLC pathway in ET_AR-low-CHO.

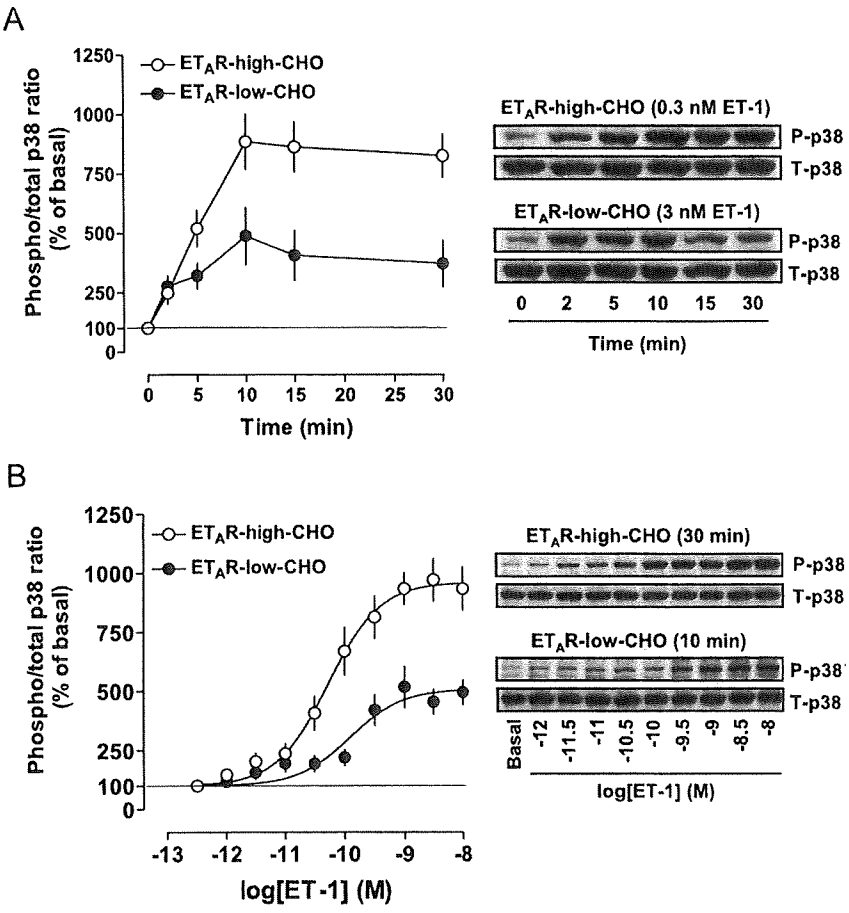

Fig. 5. Characterization of p38MAPK phosphorylation in response to ET-1 in ET_AR-high-CHO and ET_AR-low-CHO. A) Time course of p38MAPK phosphorylation induced by 0.3 nM ET-1 in ET_AR-high-CHO and by 3 nM in ET-1 in ET_AR-low-CHO with, at the right, representative immunoblots (P-p38, phosphorylated p38MAPK; T-p38, total p38MAPK). B) Concentration–response curves for p38MAPK phosphorylation in response to 30- and 10-min exposure to ET-1 in ET_AR-high-CHO and ET_AR-low-CHO, respectively, with, at the right, representative immunoblots. Data are presented as means ± S.E.M. of the results obtained from 6 experiments.

To elucidate $G_{\alpha q/11}$/PLC-independent pathways contributing to the ET-1–induced phosphorylation of p38MAPK in ET_AR-high-CHO, the possible involvement of $G_{\alpha 12}$ protein was examined using recombinant adenovirus that introduces $G_{\alpha 12}$-ct along with GFP protein into cells. Adenovirus infection at 300 MOI of CHO cells expressing ET_AR resulted in expression of recombinant GFP in approximately 90% of cells, as determined by fluorescence of GFP with flow cytometry (Fig. 7). mRNA expression for $G_{\alpha 12}$-ct was assessed by RT-PCR in either ET_AR-high-CHO or ET_AR-low-CHO after infection of recombinant adenovirus encoding $G_{\alpha 12}$-ct but not GFP (Fig. 8). Furthermore, no band corresponding to $G_{\alpha 12}$-ct was present in the PCR products without RT (data not shown). These results rule out the possibility that these fragments are non-specifically amplified products derived from contaminating genomic DNA. The effects of $G_{\alpha 12}$-ct on the ET-1–induced phosphorylation of p38MAPK were assessed by comparing the responses in GFP-expressing cells with those in $G_{\alpha 12}$-ct-expressing cells, since the $G_{\alpha 12}$-ct construct also expresses GFP (16).

The expression of $G_{\alpha 12}$-ct by adenovirus infection did not affect basal levels of p38MAPK phosphorylation in the absence of ET-1 stimulation, in either ET_AR-high-CHO or ET_AR-low-CHO. In contrast, the expression of $G_{\alpha 12}$-ct significantly inhibited the ET-1–evoked increases in levels of p38MAPK phosphorylation in ET_AR-high-CHO (Fig. 9A) but not in ET_AR-low-CHO (Fig. 9B). These results suggest that receptor-G_{12} coupling is required for activation of p38MAPK by ET-1 in ET_AR-high-CHO.

Discussion

There is considerable evidence that receptor expression level is an important determinant for coupling of receptor with G proteins. In recombinant systems, promiscuous interaction of receptors with G proteins was observed, when receptor density increased. It has been reported that G_s and G_q coupling to calcitonin receptors expressed in HEK293 cells (10) and G_i and G_s coupling to α_2-ARs expressed in CHO cells (25) are dependent on the receptor expression level. Such multiple coupling of receptors to G proteins is speculated to induce differential cellular responses to an agonist acting on the same receptor. The present study compared the signal transduction pathways utilized by human ET_AR expressed in

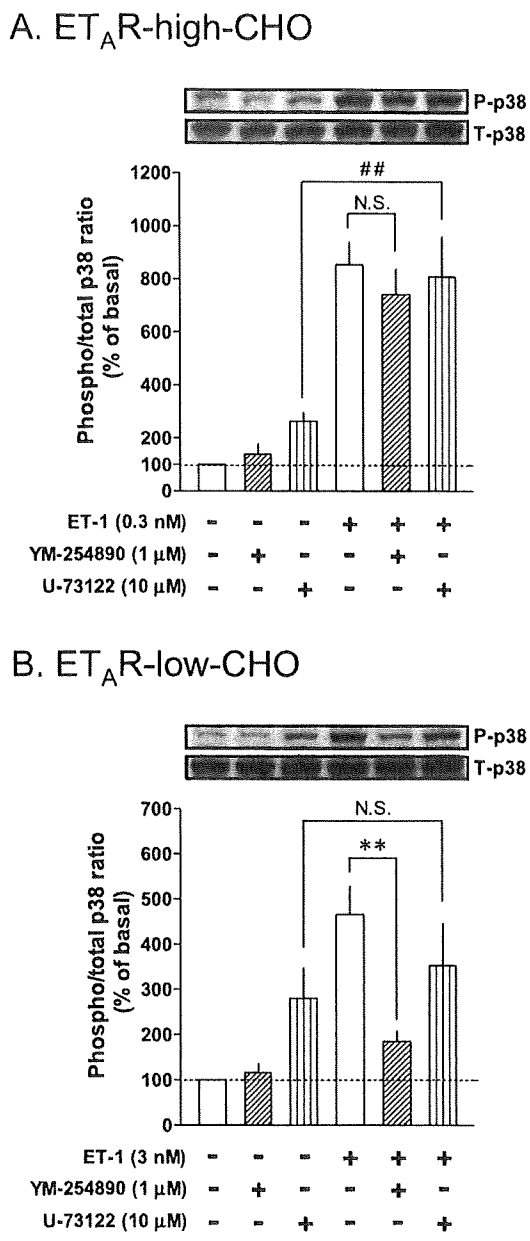

Fig. 6. Effects of YM-254890 and U-73122 on p38MAPK phosphorylation in response to 30-min exposure to 0.3 nM ET-1 in ET_AR-high-CHO (A) and to 10 min exposure to 3 nM ET-1 in ET_AR-low-CHO (B). The cells were treated with the inhibitors for 30 min before stimulation with ET-1. Data are presented as means ± S.E.M. of the results obtained from 6 experiments. $^{\#\#}P<0.01$, between both groups indicated. $^{**}P<0.01$, vs. its control (3 nM ET-1 alone). N.S., not significant between the indicated columns.

CHO cells at different levels (referred to as ET_AR-high-CHO and ET_AR-low-CHO in this paper) to clarify the functional significance of receptor density in determining the coupling of ET_AR to G_q and G_{12} proteins and its down-stream signaling cascades.

The potency of ET-1 in inducing transient $[Ca^{2+}]_i$ increases was approximately 20-fold higher in ET_AR-high-CHO than in ET_AR-low-CHO, although the binding affinity of [^{3}H]BQ123 for ET_AR in both cell lines was similar to each other. This finding clearly indicates that an increase in ET_AR expression level leads to changes in the efficacy of ET-1. Alternations in agonist potency or efficacy are reported to be frequently accompanied by activation of multiple signaling pathways (26).

In ET_AR-high-CHO, high concentrations of ET-1 induced an increase in $[Ca^{2+}]_i$ consisting of two phases, a transient phase and a subsequent sustained phase, as reported previously (6). It is generally thought that the initial Ca^{2+} signal phase (produced by G_q protein–coupled receptors) is generated by IP_3-dependent Ca^{2+} release from the intracellular Ca^{2+} store and that the resulting depletion of the Ca^{2+} store triggers activation of store-operated Ca^{2+} channels (SOCCs), leading to the sustained $[Ca^{2+}]_i$ increase (27, 28). However, such a scheme in which development of ET-1–induced sustained phase is dependent on its initial $[Ca^{2+}]_i$ increase cannot provide an entirely satisfactory explanation for our results obtained in ET_AR-high-CHO and ET_AR-low-CHO, since the amplitude of sustained Ca^{2+} influx evoked by ET-1was not correlated with that of the initial increases in $[Ca^{2+}]_i$. That is, although the transient $[Ca^{2+}]_i$ increases induced by 0.3 nM ET-1 in ET_AR-high-CHO and by 3 nM ET-1 in ET_AR-low-CHO are comparable with each other (Fig. 2), the amplitude of the sustained Ca^{2+} responses to ET-1 was markedly different in these two types of cells. These findings suggest that the ET-1–induced sustained Ca^{2+} influx in ET_AR-high-CHO is not due to SOCCs operated by the emptying of the intracellular Ca^{2+} store (29, 30). Key candidates for such SOCC-independent pathways are NSCCs (1) and NHE (7), both of which are reported to be activated by GPCRs. Regarding NSCCs, it has been suggested that both G_q and G_{12} proteins are necessary for activation of these channels by ET_AR in CHO cells overexpressing ET_AR, although the receptor density of the cells is not determined (1, 2). In ET_AR-high-CHO and ET_AR-low-CHO, ET_AR is considered to be coupled with $G_{q/11}$ protein, judging from the sensitivity of the ET-1–induced transient increases of $[Ca^{2+}]_i$ in both cell lines to a $G_{aq/11}$ inhibitor (YM-254890) and a PLC inhibitor (U-73122) (data not shown) and from the sensitivity of the sustained increases in ET_AR-high-CHO to these inhibitors (Fig. 3). Based on these data, we assumed that the difference of sustained Ca^{2+} influx in ET_AR-high-CHO and ET_AR-low-CHO is due to different efficiency of coupling of ET_AR to G_{12} protein, which in turn depends on the expression level of ET_AR. Namely, in ET_AR-low-CHO, ET-1 could not activate G_{12}-mediated signaling pathways, failing to induce sustained Ca^{2+}